MASTER'S THESIS

Master of Science in Advanced Mathematics and Mathematical Engineering

Title: Synchronization Properties of Neuronal Oscillators and Memristor Devices

Author: Jose Segura Díaz

Advisor: Gemma Huguet Casades

Department: Mathematics

Academic year: 2018

UNIVERSITAT POLITÈCNICA DE CATALUNYA
BARCELONATECH
Facultat de Matemàtiques i Estadística

Universitat Politècnica de Catalunya
Facultat de Matemàtiques i Estadística

Master in Advanced Mathematics and Mathematical Engineering

Master's thesis

Synchronization Properties of Neuronal Oscillators and Memristor Devices

Jose Segura Díaz

Supervised by Gemma Huguet Casades

May, 2018

I would like to thank my advisor, Dr. Gemma Huguet,
for all her help and constant support.

Abstract

Neuromorphic computation (inspired by neuroscience) aims to develop electronic devices that emulate neuronal activity in order to develop new paradigms of computation beyond digital machines. In this project, we develop a new model for circuits with memristic devices (inspired by neuronal models) showing oscillatory dynamics and we apply the classical theory for weakly coupled oscillators to study the dynamics for coupled memristic devices. First, we review the general theory and show its application to coupled neuronal oscillators, Finally, we consider different combinations of couplings for memristic devices to predict different synchronization outcomes and its relevance for practical applications.

Keywords

neuronal models, memristic device, hysteresis, oscillators, synchronization, weak coupling, phase resetting curves, numerical computation

Contents

1 Introduction

The fast growth in technology and informatics has led to a high demand for new devices for computation, increasingly faster and with more capacity. Nowadays, a common trend in innovation is to use concepts inspired by the human brain, such as the famous neuronal networks for data science. Neuron-inspired devices for computation are the electronic oscillators, which have an important role in the generation of many computer tasks such as clock signal generation or signal broadcast for communications.

Recent advances in nanotechnology are used to emulate the oscillatory activity of a neuron. In particular memristic devices can emulate the behavior of synapses. Such devices are nanoscale realizations of a new type of electrical component called "memristor". The memristor, envisioned by Leon Chua in 1971, presents different resistance values depending on the history of electric charge that has flowed through it—it has "memory". Phase change materials are emerging as excellent candidates to implement memristic devices because they have a different resistance value associate to each phase, and the phase can be controlled through electrical fields. Materials based on Vanadium Dioxide (VO_2) present an interesting characteristic that approximates the memristor: hysteresis. Its resistance can switch between two values depending not only on the current values of voltage, but also the values in the past. Due to the hysteresis, an oscillator can be constructed, consisting of connecting a $V0_2$ terminal with an electrical resistor and a capacitor. Experimental simulations have been done in order to describe its dynamics [1, 2, 3], and a model has been proposed [4]. The objective of these papers is to find a new component that can be used for computation in a different way that our common processors. So a question arises: Can these oscillators exchange "information"? Or in other words, can one device be affected by the oscillation of another, or even synchronize to it? The models of the memristic circuits can be studied in order to find an answer to this question.

In this project we propose an alternative modelling based on neuron models such as the Hodgkin-Huxley or the Morris-Lecar models. Inspired by the modelling of neuron's ion channels, the main idea is introduce an equation governing the resistance of the memristor device that can emulate the hysteresis observed experimentally. We show that the model proposed shows oscillations as certain parameters of the model are varied.

Models for neurons have been widely studied, specially their oscillatory behaviour and synchronization properties when coupled [5, 6]. Many methods and tools have been developed to study their dynamics, such as the Phase Resetting Curve (PRC). The PRC describes the change in the cycle period of an oscillator induced by a perturbation as a function of the phase at which it is received. The PRC is then used to reduce the study of the dynamics on the oscillator when the coupling is weak. This theory has been extensively applied to study coupled neuronal oscillators with specific software designed for it [7]. In this project we will review the classical theory for coupled oscillators and its applications to neuronal models. Finally, we will apply it to study the dynamics of coupled memristic oscillators. Our ultimate goal would be to determine if synchronization if possible, and under which circumstances.

The project is organized as follows. In section 2, we describe two common models for neurons and the couplings between them. In section 3, we present our model for a memristic device, we study its oscillatory dynamics and propose several ways to couple them. In section 4, we introduce the phase resetting curve (PRC) and the general theory for weakly coupled oscillators to study synchronization. We also include a description of the numerical methods to compute the functions involved. Finally, in section 5, we apply the methods presented to the model for memristic devices proposed in section 2.

2 Neuronal Models

In this section we review the classical models for neurons and connections between neurons (synapses) that will be used along the document to illustrate the theory of weakly coupled oscillators.

2.1 The Hodgkin–Huxley Equations

Alan Lloyd Hodgkin and Andrew Fielding Huxley proposed a model in 1952 for the action potential (rapid changes in the membrane voltage, see Figure 1) of the squid giant axon that has become the paradigm for a quantitative description of the electrical activity of the neurons. They received the 1963 Nobel Prize in Physiology or Medicine for this work.

The typical Hodgkin–Huxley model treats each component of an excitable cell as an electrical element of an electrical circuit (as shown in Figure 2). The dynamics of this circuit models the action potential (see Figure 1) characteristic of a neuron. The neuron's membrane is modeled as a capacitor with capacitance C. Voltage-gated ion channels embedded in the membrane are modeled as resistors with conductances g_{Na}, g_K, corresponding to the sodium and potassium voltage-gated ionic channels, respectively. Other ionic channels are represented by resistors with constant conductances g_L. The electrochemical gradients driving the flow of ions through the ionic channels are represented by voltage sources (V_{Na}, V_K, V_L) whose voltages are determined by the ratio of the intra- and extracellular concentrations of the ionic species of interest. Finally, external inputs are represented by current sources (I). The membrane potential is denoted by V.

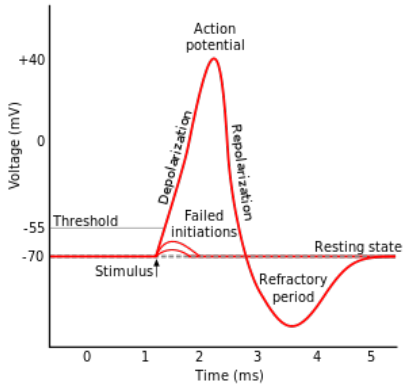

Figure 1: Action potential of a neuron. Figure from *Wikipedia*.

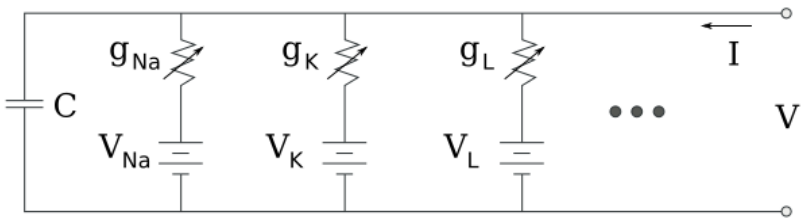

Figure 2: Circuit of a Hodgkin-Huxley model.

Using a series of voltage clamp experiments and by varying extracellular sodium and potassium concentrations, Hodgkin and Huxley developed a model in which the properties of an excitable cell are described

by a set of four ordinary differential equations given by

$$\begin{aligned} C\frac{\mathrm{d}V}{\mathrm{d}t} &= -\bar{g}_{\mathrm{K}}n^4(V-V_K) - \bar{g}_{\mathrm{Na}}m^3h(V-V_{Na}) - \bar{g}_L(V-V_L) + I, \\ \frac{dn}{dt} &= \alpha_n(V)(1-n) - \beta_n(V)n, \\ \frac{dm}{dt} &= \alpha_m(V)(1-m) - \beta_m(V)m, \\ \frac{dh}{dt} &= \alpha_h(V)(1-h) - \beta_h(V)h, \end{aligned} \tag{1}$$

where I is the current per unit area, and α_i and β_i are the rates at which the i-th ionic channel opens and closes, respectively. The variables n, m, and h are dimensionless quantities between 0 and 1 that are associated with potassium channel activation, sodium channel activation, and sodium channel inactivation respectively.

The system is nonlinear and cannot be solved analytically. However, there are many numerical methods available to analyze the system. Indeed, we know that changes in the parameter I show transitions from an equilibrium to a periodic orbit. For this project, we will use an equivalent 2-dimensional model known as the Morris-Lecar model.

2.2 The Morris-Lecar Equations

The Morris-Lecar (ML) model is a 2-dimensional model developed by Catherine Morris and Harold Lecar (1981) from experiments with barnacle giant muscular fibers, which showed different kinds of oscillation.

The ML model equations are:

$$\begin{aligned} C\dot{V} &= -g_{Ca}m_\infty(V)(V-E_{Ca}) - g_K w(V-E_K) - g_L(V-E_L) + I_{app}, \\ \dot{w} &= \phi\frac{w_\infty(V)-w}{\tau_\infty(V)}, \end{aligned} \tag{2}$$

where g_{Ca}, g_K are the intrinsic conductances of calcium and potassium, respectively, g_L is the leak conductance, E_{Ca}, E_K and E_L are the respective reversal potential. The variable $w \in [0,1]$ is the probability that the potassium channel opens.

The functions m_∞, w_∞ and τ_∞ are defined as:

$$\begin{aligned} m_\infty(V) &= (1+\tanh((V-V_1)/V_2))/2, \\ w_\infty(V) &= (1+\tanh((V-V_3)/V_4))/2, \\ \tau_\infty(V) &= (\cosh((V-V_3)/(2V_4)))^{-1}. \end{aligned} \tag{3}$$

For this project, unless stated differently the parameters used for the ML model are:

$$\begin{array}{cccc} E_L=-60, & E_K=-84, & E_{Ca}=120 & (\text{in mV}), \\ V_1=-1.2, & V_2=18, & V_3=12, & V_4=17, \\ gL=2, & g_K=8.0, & g_{Ca}=4, & (\text{in mS}/cm^2), \\ C=20\ \mu F/cm^2, & \phi=0.66667, & I_{app}=80\ A. & \end{array} \tag{4}$$

2.3 Synapse: The synaptic activation equation

In order to study the interaction between two neurons, we must include in our previous equations the effect of the synaptic current between them. In the nervous system, a synapse (see Figure 3) is a structure that permits a neuron, called presynaptic, to pass an electrical or chemical signal in the form of neurotransmitters to another neuron, called postsynaptic.

We model the synaptic current as

$$I_{syn} = g(t)(V_{post} - V_{syn}).$$

We can define the conductance $g(t) = \bar{g}s(t)$, where $s(t)$ denotes the fraction of open channels, taking values between 0 and 1. Here, $s(t)$ satisfies

$$\dot{s} = \alpha K(V)(1 - s) - \beta s,$$

where K denotes the concentration of transmitter released into the synaptic cleft by a presynaptic neuron, modelled by

$$K(V) = 1/(1 + exp(-(V - V_t)/V_s)).$$

There are two types of synapses. The **excitatory** synapses in which an action potential in a presynaptic neuron increases the probability of an action potential occurring in a postsynaptic cell and the **inhibitory** synapses in which an action potential in a presynaptic neuron decreases the probability of an action potential occurring in a postsynaptic cell. We model them in the following way:

- **Excitatory** when $-(V_i - V_{syn}) > 0$ (e.g. $V_{syn} = 120V$, since V_i typically ranges between -70 and -20 mV).

- **Inhibitory** when $-(V_i - V_{syn}) < 0$ (e.g. $V_{syn} = -75V$, since V_i typically ranges between -70 and -20 mV).

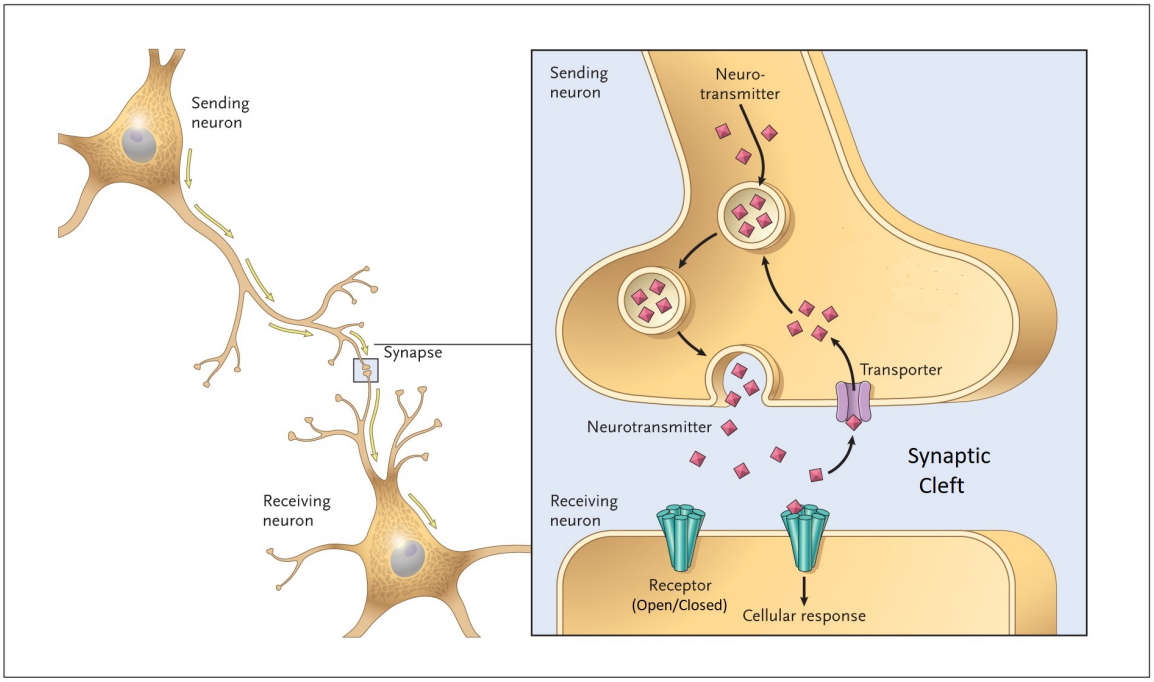

Figure 3: Schematic of the synapse between two neurons. Image from *Wikimedia*.

In this project we will use the Morris Lecar model to model the activity of several neurons coupled using the activation synapse described in Figure 3. The resultant model for n identical neurons fully connected with the same kind of coupling will be, for $i = 1...n$:

$$\begin{aligned} C\dot{V}_i &= -g_{Ca}m_\infty(V_i)(V_i - E_{Ca}) - g_K w_i(V_i - E_K) - g_L(V_i - E_L) - \bar{g}\sum_{\substack{1\le j\le n \\ j\neq i}} s_j(V_i - V_{syn}) + I_{app}, \\ \dot{w}_i &= \phi\frac{w_\infty(V_i) - w_i}{\tau_\infty}, \\ \dot{s}_i &= \alpha K(V_i)(1 - s_i) - \beta s_i. \end{aligned} \tag{5}$$

3 Memristor Devices

A memristor (a portmanteau of memory resistor) is a hypothetical electrical component envisioned in 1971 by circuit theorist Leon Chua. According to the characterizing properties, the memristor would operate in the following way: memristor's electrical resistance is not constant but depends on the history of current that has previously flowed through the device, i.e., its present resistance depends on how much electric charge has flowed in what direction through it in the past.

In 2008, a team at HP Labs claimed to have found the first memristor based on an analysis of a thin film of titanium dioxide thus connecting RAM devices to the memristor concept. The HP result was published in the scientific journal Nature [8].

An approach to this concept is shown in papers like [4] where they propose a model with Vanadium Dioxide devices, which their main features are (see Figure 4): First, a switching-like behaviour with large and abrupt change in electrical conductivity that can be triggered by the applied electrical voltage. Secondly the presence of a hysteresis in that behaviour driven by two different voltage values. The hysteresis is the characteristic that allows the device to have a different values of resistance depending on the values of voltage of the past, because the triggering voltage for the resistance change will depend if the voltage was decreasing or increasing.

In this project we propose a model based on the hysteretic behaviour of these vanadium devices, which will be called from now on *"memristic devices"* or just *"memristors"*, despite not having full memristor properties and only an approximation to them.

3.1 The relaxation oscillator

In electronics a relaxation oscillator is a nonlinear electronic oscillator circuit that produces a nonsinusoidal repetitive output signal. It achieves its repetitive behavior from the charging of a capacitor to some event threshold. The event discharges the capacitor, and its recharge time determines the repetition time of the events.

We consider the circuit presented in Figure 4 consisting of a memristic device with non-constant resistance $R_M(t)$, a resistor, with constant resistance R_S, and a capacitor, with capacitance C.

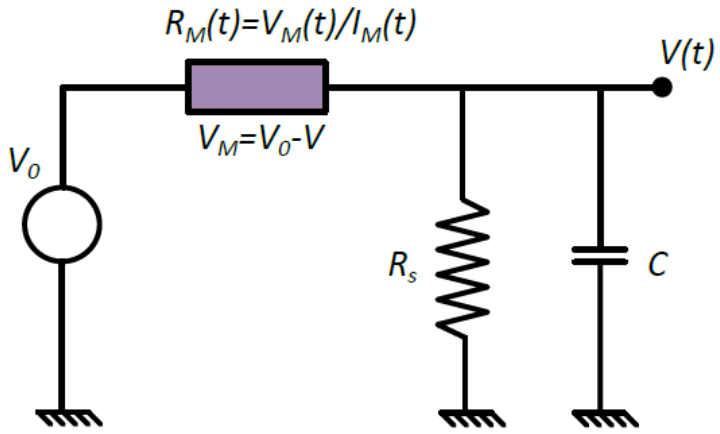

Figure 4: Schematic representation of circuit.

The equation for voltage V(t) can be obtained by applying the Kirchhoff's law to the circuit, and is given by:

$$C\dot{V} = \frac{V_0 - V}{R_M} - \frac{V}{R_s}$$

The memristor with resistance R_M can take values between R_l (the minimum) and R_h (the maximum).

We study here the case where the memristor takes a high value of resistance, R_h at high voltages and a low resistance value, R_l, at low voltages (see Figure 5).

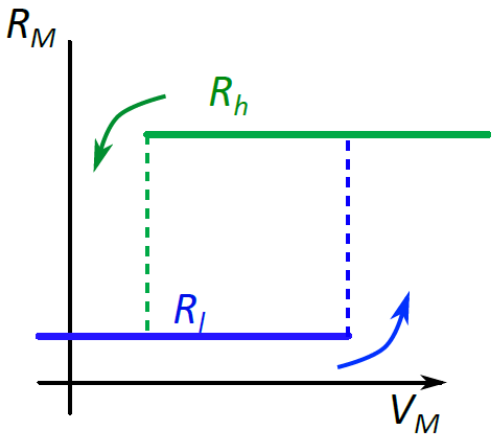

Figure 5: Resistance behaviour of the memristic device. The memristor can take values between R_l (the minimum) and R_h (the maximum). Notice the hysteresis phenomenon causing two values of voltage where there is a switch.

In Maffezzoni et al. (2015) [4] the authors study the dynamics of a single oscillator and the coupling of two of them by considering that the memristor can only take 2 values, R_l and R_h and they are reached instantaneously (or much faster than the rest of the circuit dynamics).

Note that if we freeze the memristor resistance at $R_M = R^*$ where $R^* = R_h$ or $R^* = R_l$ the equation for V becomes

$$C\dot{V} = \frac{R_s + R^*}{R_s R^*}(-V + \frac{R_s V_0}{R_s + R^*}).$$

and defining $\tau_V = C\frac{R_s R^*}{R_s + R^*}$ and $\bar{V} = \frac{R_s V_0}{R_s + R^*}$, we are left with the linear system

$$\dot{V} = \frac{1}{\tau_V}(-V + \bar{V}),$$

where V will tend exponentially to the value $\bar{V}$ with a time constant τ_V . Notice that the time constant for V depends on the capacitance C, the resistance R_s and the memristor's resistance R. The solution can be computed analytically:

$$V(t) = \bar{V} + (V(0) - \bar{V})e^{-t/\tau_V}.$$

Note that if $Rs << R^*$ (for instance $R^* = R_h$) then $\tau_V \approx CR_s$ and if $R_s \approx R^*$ (for instance $R^* = R_l$) then $\tau_V \approx CR_s/2$. Thus, V raises faster than it decays. This effect was measured and described in [4].

3.2 Our model for the memristor device

Previous works have modeled of the memristor dynamics —with hystheretic behavior— with a driving point equivalent circuit. Such modeling consists of having the memristor state controlled by a voltage

comparator that computes a function that depends on the applied voltage and the current resistance state. There is a time constant applied to the circuit that is based on the phase transition detected in laboratory measurements. However, those works consider memristic dynamics to be much faster compared with the one given by the oscillator circuit elements and thus the model only considers possible memristor values of R_h and R_l and disregards the memristic dynamics. Our modeling aims at considering the memristic dynamic as an important part of the memristor oscillator. We first consider an equation for the memristor resistance, R,

$$\tau_\theta \dot{R} = -R + F(V_M, R), \tag{6}$$

where τ_θ is a time constant associated to the switching time of the memristor and $F(V_M, R)$ is a function that determines the resistance value the memristor tries to reach at a given voltage. $V_M = V_0 - V$ is the voltage across the memristor. F must depend not only on the applied voltage to the memristor but also on its resistance value in order to have hysteresis.

First let us consider the function

$$f(x) = R_l + (R_h - R_l)\frac{1}{1 + \exp[\alpha x]}$$

which basically takes values of R_l when $V > 0$ and R_h when $V < 0$ (See Figure 6-left). Next we introduce a dependence on the memristor state for the function f so that there is hysteresis. We consider the argument of the function f as $x = -c_1 R + c_2 + V_M$. Therefore we define F as:

$$F(V_M, R) = f(-c_1 R + c_2 + V_M). \tag{7}$$

The constant c_1 is in units of current and c_2 is in units of voltage transforms the state R_h and R_l into voltages such that $V_l = c_1 R_l + c_2$ and $V_h = c_1 R_h + c_2$ that are the switching voltages for the sweep up and sweep down respectively. Figure 6 (right) shows the nullcline of the memristor resistance, obtained by equating (6) to zero. Notice the hysteresis that is introduced and that will produce our desired effect, explained in the next section.

If we add the usual equation for the voltage, we obtain the model for the circuit in Figure 6

$$\begin{aligned} C\dot{V} &= \frac{V_0 - V}{R} - \frac{V}{R_s} \\ \tau_\theta \dot{R} &= -R + f(-c_1 R + c_2 + V_0 - V) \\ f(x) &= R_l + (R_h - R_l)\frac{1}{1 + \exp[\alpha x]}. \end{aligned} \tag{8}$$

For this model, unless stated differently, we will use the following parameters:

$$\begin{array}{lll} C = 1F, & \tau = 1.5, & V_0 = 20V, \\ R_s = 20\Omega, & R_h = 100\Omega, & R_l = 10\Omega, \\ c_1 = 0.08A, & c_2 = -8V, & \alpha = 125V^{-1}. \end{array} \tag{9}$$

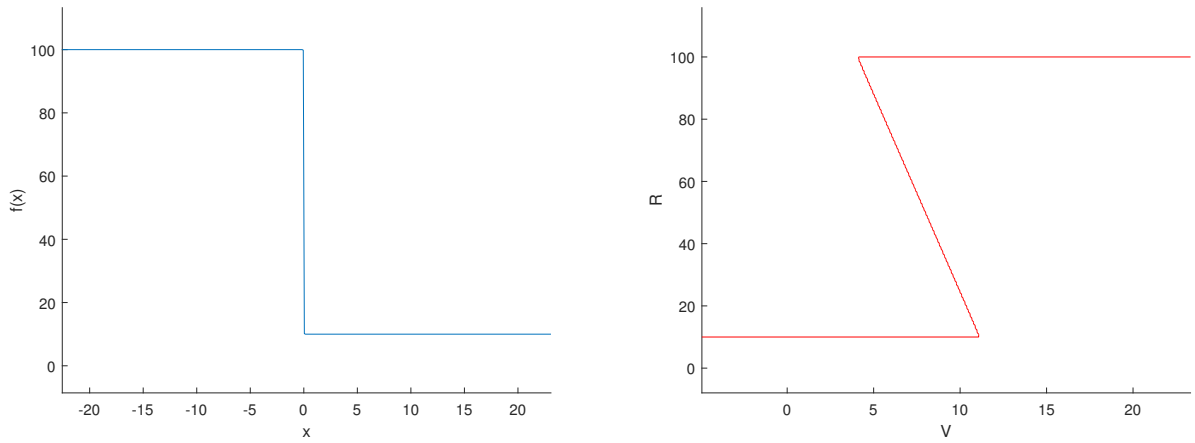

Figure 6: For $\alpha = 125$, $R_h = 100$, $R_l = 10$. Left: Plot of $f(x)$. Right: Nullcline of the memristor resistance for $c_1 = 0.08$, $c_2 = -8$.

3.3 Stability and bifurcations

In this section we provide a description of the dynamics of the memristor model in (8). Notice that the system shows a *slow-fast* dynamics, since it has variables evolving at different time scales. Moreover, as parameters V_0 and R_s are varied, the system undergoes several bifurcations, some of them giving rise to periodic orbits. If we take a look at the nullclines of system (8) using the set of parameters (9) but varying R_s and V_0 (see Figure 7) we find that the equilibrium points (i.e. the intersection between nullclines) appear in different regions. Figure 8 shows bifurcations diagrams as V_0 varies (left) and R_s varies (right). Both diagrams present three separated regions: a region with a unique stable fixed point for the small and large values of the parameter, a region where there is a unique equilibrium point which is unstable, and a small region where three equilibrium points appear, two unstable and one stable.

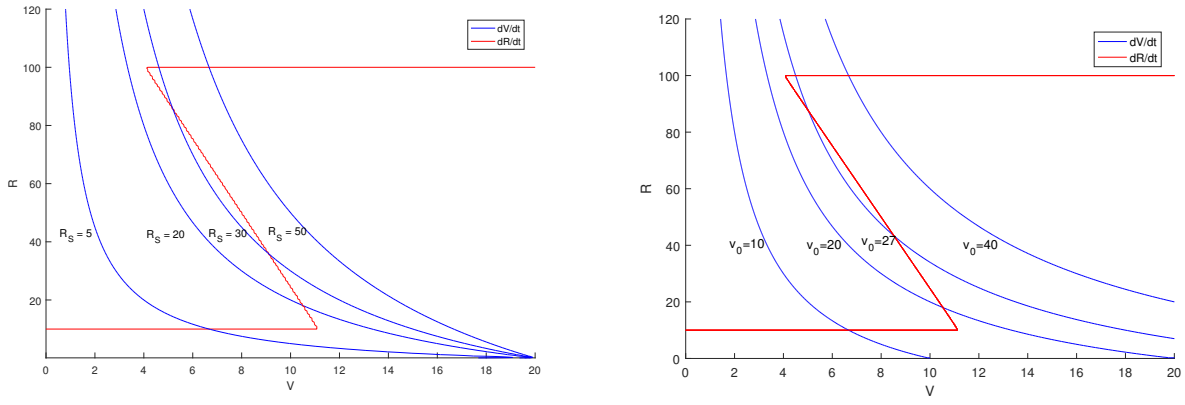

Figure 7: Nullclines of the memristor model for some values of R_s (left) and V_0 (right).

In the bifurcation diagram a stable focus changes stability and becomes unstable at a **Hopf bifurcation**

and a periodic solution arises (see Fig 9). There is more information about bifurcations in Appendix A. The periodic solution is born with small amplitude but but soon it expands to occupy all the shape of the resistance nullcline. This fast transition is called the *Canard phenomenon*. The shape of the orbit is the expected outcome because resistance will be most of the time at the R_l or R_h values, and its transition will be very fast.

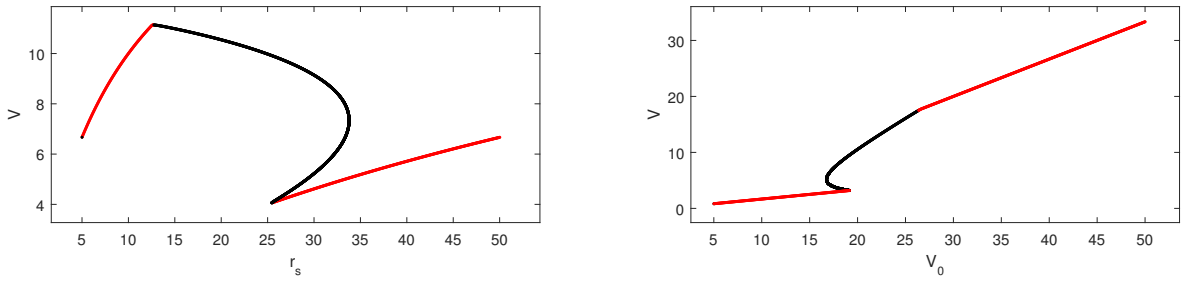

Figure 8: Bifurcation diagram for the parameters R_s (left) and V_0 (right) of system (8). Stable equilibrium points in red, unstable in black.

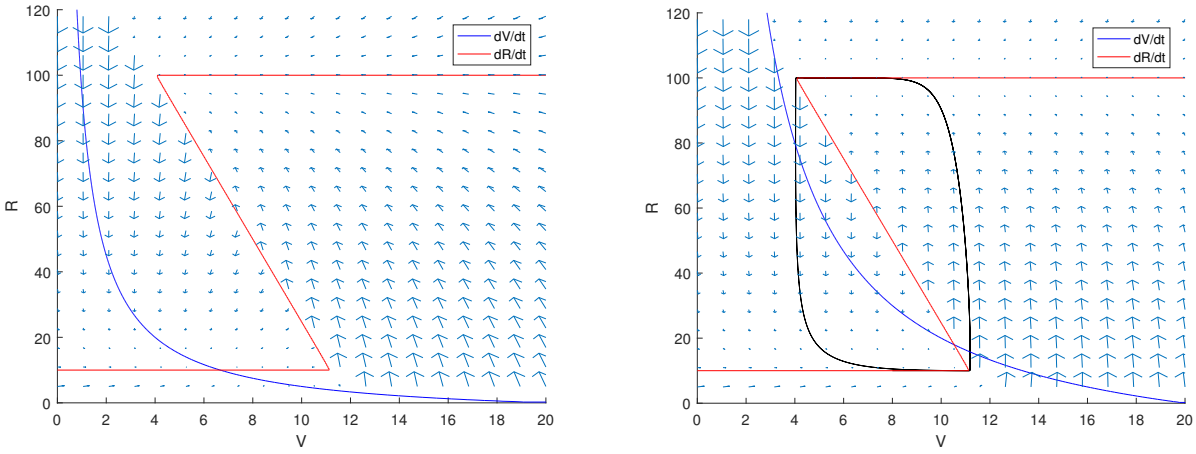

Figure 9: Left : Fixed point for $R_s = 5$ and $V_0 = 20$. Right: Periodic orbit for $R_s = 20$ and $V_0 = 20$.

3.4 Coupling memristors

As in neurons, in order to study the dynamics between two coupled memristor circuits, we describe two possible couplings between them (see Figure 10).

- Using a **resistor** with resistance $R_\epsilon = \frac{1}{\epsilon}$. This model consists of connecting the circuits with a

resistance between them (see Figure 10 top). We can calculate the resulting model as:

$$\begin{aligned} C\dot{V}_1 &= \frac{V_0 - V_1}{R_1} - \frac{V_1}{R_s} + \epsilon(V_2 - V_1), \\ \tau_\theta \dot{R}_1 &= -R_1 + f(V_1, R_1), \\ \bar{C}\dot{V}_2 &= \frac{\bar{V}_0 - V_2}{R_2} - \frac{V_2}{\bar{R}_s} + \epsilon(V_1 - V_2), \\ \bar{\tau}_\theta \dot{R}_2 &= -R_2 + f(V_2, R_2). \end{aligned} \tag{10}$$

- Using a **capacitor** with capacitance $C_\epsilon = \frac{1}{\epsilon}$ (see Figure 10 bottom). With this coupling derivatives appear on the right hand side:

$$\begin{aligned} C\dot{V}_1 &= \frac{V_0 - V_1}{R_1} - \frac{V_1}{R_s} + \epsilon(\dot{V}_2 - \dot{V}_1), \\ \tau_\theta \dot{R}_1 &= -R_1 + f(V_1, R_1), \\ \bar{C}\dot{V}_2 &= \frac{\bar{V}_0 - V_2}{R_2} - \frac{V_2}{\bar{R}_s} + \epsilon(\dot{V}_1 - \dot{V}_2), \\ \bar{\tau}_\theta \dot{R}_2 &= -R_2 + f(V_2, R_2). \end{aligned} \tag{11}$$

In order to study the model, we will substitute on the right hand side the derivatives by $\dot{V}_i = \frac{1}{C}\frac{V_0 - V_i}{R_i} - \frac{V_i}{R_s} + \epsilon(\dot{V}_j - \dot{V}_i)$ and neglect terms of order ϵ^2.

$$\begin{aligned} C\dot{V}_1 &= \frac{V_0 - V_1}{R_1} - \frac{V_1}{R_s} + \epsilon\left[\frac{1}{\bar{C}}\left(\frac{\bar{V}_0 - V_2}{R_2} - \frac{V_2}{\bar{R}_s}\right) - \frac{1}{C}\left(\frac{V_0 - V_1}{R_1} - \frac{V_1}{R_s}\right)\right] + \mathcal{O}(\epsilon^2), \\ \tau_\theta \dot{R}_1 &= -R_1 + f(V_1, R_1), \\ \bar{C}\dot{V}_2 &= \frac{\bar{V}_0 - V_2}{R_2} - \frac{V_2}{\bar{R}_s} + \epsilon\left[\frac{1}{C}\left(\frac{V_0 - V_1}{R_1} - \frac{V_1}{R_s}\right) - \frac{1}{\bar{C}}\left(\frac{\bar{V}_0 - V_2}{R_2} - \frac{V_2}{\bar{R}_s}\right)\right] + \mathcal{O}(\epsilon^2), \\ \bar{\tau}_\theta \dot{R}_2 &= -R_2 + f(V_2, R_2). \end{aligned} \tag{12}$$

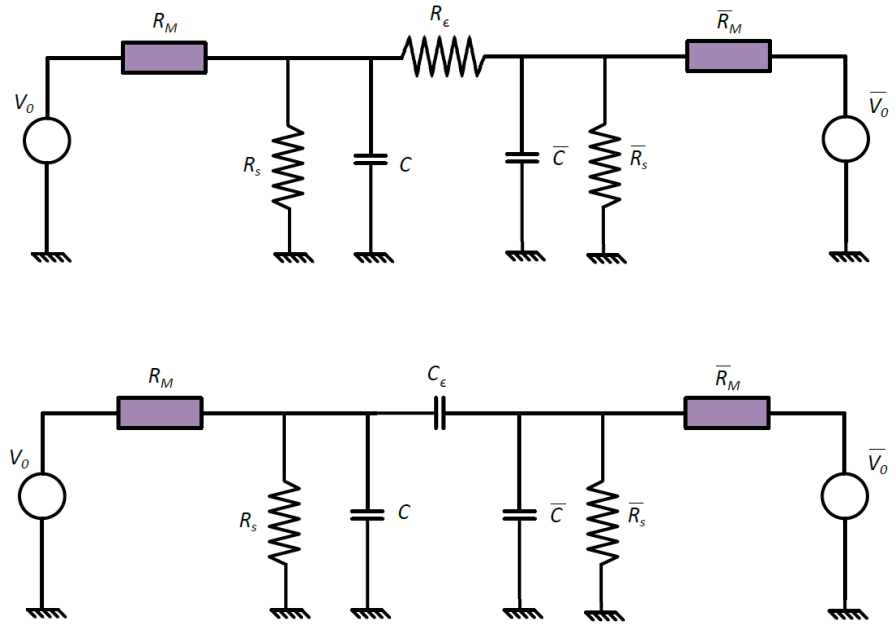

Figure 10: Two types of coupling between memristor circuits. On top, using a resistor. On the bottom, using a capacitor.

4 Neural Oscillators

In this section we will review the classical theory for weakly coupled systems and we will show how it can successfully predict synchronization properties for coupled neurons. We consider a system of n coupled neurons, that each individual neuron, when uncoupled, oscillates.

4.1 The Phase Resetting Curve (PRC)

Since each neuron when uncoupled is oscillating, this corresponds to an oscillator subject to an external perturbation (which corresponds to the effect of the coupling from other neurons). The simplest case will be observing how the firing time of a single neuron changes when given an immediate perturbation. A more complex study will allow us to see groups of neurons interacting with each other with behaviour such as synchronization.

Consider the general case of the system of differential equations in $\mathbb{R}^n$

$$\frac{dX}{dt} = F(X), \tag{13}$$

having a limit cycle Γ of period T. A limit cycle is an isolated periodic orbit.

The limit cycle is said to be orbitally asymptotically stable if nearby initial conditions approach Γ as $t \to \infty$. We can parametrize Γ by time and thus define a phase, $\phi \in [0, T)$, along the limit cycle. Let $\Theta(x)$ denote the phase of the oscillator for a point x on Γ. When the limit cycle is hyperbolic, it is possible to define a phase for points y in a neighborhood of the cycle [9]. Let $X(t; y)$ be the solution of (13) with initial condition y. Suppose y is a point in the neighborhood of the limit cycle, then there exists x on the limit cycle ($x \in \Gamma$) such that $||X(t; x) - X(t; y)|| \to 0$ as $t \to \infty$. Then we define $\Theta(y) = \Theta(x)$ as the **asymptotic phase** of y. That is, as $t \to \infty$, the solutions are indistinguishable.

Definition 4.1. *The set of points y which have the same asymptotic phase $\Theta(x)$ is called the* **isochron** *of a point $x \in \Gamma$, which will be denoted as $N(x)$.*

Isochrons are invariant sections for the map at time T, $X(T, \cdot)$, where T is the period of the limit cycle (see Figure 11 left); that is, for a point $y \in N(x)$, $X(T; y) = y' \in N(x)$. Of course, the existence of isochrons is related to the asymptotic phase, $\Theta(x)$.

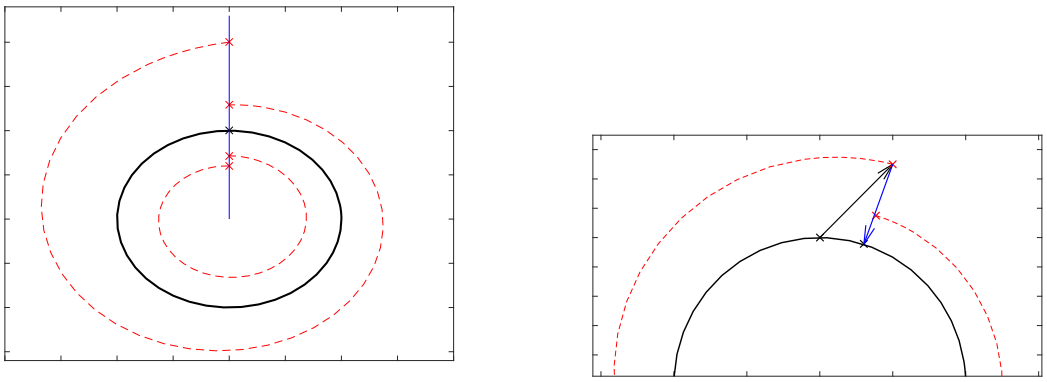

Figure 11: (Left) In blue, the isochron of a point of a periodic orbit. We can see some trajectories of points on the isochron that return to it after a time T equal to the period of the orbit. (Right) Effect of a perturbation onto the phase. The trajectory is displaced (black arrow) to a point off the limit cycle, which belongs to a different isochron. The point then returns to the limit cycle approaching the orbit of another point determined by the isochron.

Suppose that $\phi = \Theta(x)$ is the phase of an oscillator at point $x \in \Gamma$ and we apply a perturbation to the point x so that it is sent to a point y that belongs to the isochron of x' such that $\Theta(x') = \phi'$ for ϕ'. Then, the phase of the oscillator is reset to a different value (see Figure 11 right).

Definition 4.2. *The map from the old phase ϕ to the new phase ϕ' is called the* **phase transition curve** *(PTC), $\phi' = P(\phi)$.*

Definition 4.3. *The* **phase resetting curve** *(PRC), is defined as the difference between the new phase and the old phase:*

$$\Delta(\phi) = \phi' - \phi = P(\phi) - \phi.$$

The PRC tells us that:

- If $\Delta(\phi) < 0$: The stimulus will delay the phase ("It slows down the oscillation").
- If $\Delta(\phi) = 0$: The stimulus will not affect the phase.
- If $\Delta(\phi) > 0$: The stimulus will advance the phase ("It speeds up the oscillation").

Combining the mentioned properties and experimental results, Hansel et al. (1995) [10] identified two types of neural phase resetting curves: in **Type I** a small depolarization produced by excitatory postsynaptic potentials can only advance the phase, whereas in **Type II** either an advance or delay could be produced depending upon the timing of the perturbation.

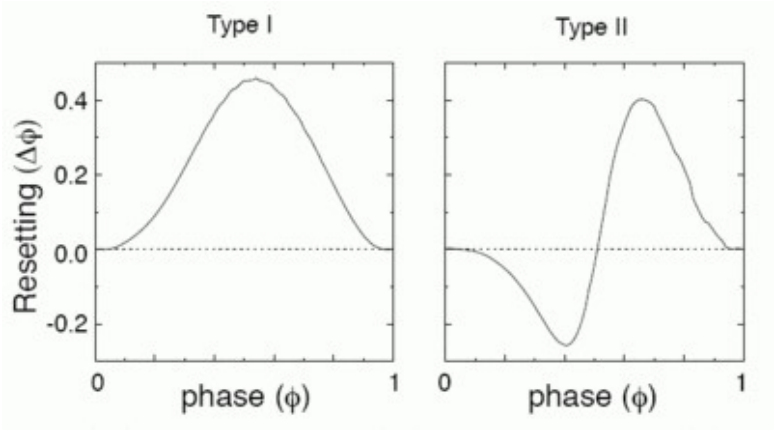

Figure 12: Two types of PRC. Image from *Scholarpedia*

It is customary to normalize the phase so that it ranges between 0 and 1 or between 0 and 2π. Therefore, we have to rescale by multipling by $1/T$ or $2\pi/T$. This is useful if we want to compare the PRCs for oscillators with different frequencies. Since this is not the case for the most part of this project, PRCs will not be normalized unless stated otherwise. Because of that, ϕ and t will be used indistinctly in this project, only different in their meaning of "phase" and "time".

We now can relate the PRC to the phase function $\Theta(x)$ defined by the isochrons of an attracting limit cycle. Let x be a point on the limit cycle, with phase (time) $\phi \in [0, T)$, i.e. $x = X^\Gamma(\phi)$. Note that $\Theta(x) = \phi$ by definition. Consider an arbitrary perturbation, $y \in \mathbb{R}^n$; of the vector field. The new phase is

$$\phi' = \Theta(x + y) = \phi + \nabla_x \Theta(x) \cdot y + O(|y|^2).$$

Thus, for small perturbations

$$\phi' - \phi = \Delta(\phi, y) = \nabla_x \Theta(x) \cdot y + O(|y|^2).$$

Suppose that we add a perturbation to a neuron on the voltage direction, corresponding to its first component, such that $y = (a, 0, ..., 0)$. Then the PRC can be approximated by the first component of the gradient of the phase function Θ evaluated at $X^\Gamma(\phi)$. That gradient is commonly called the **Z function or infinitesimal PRC (iPRC)**, as introduced by Kuramoto [11]. It provides a description of how infinitesimal perturbations of the limit cycle change its phase:

$$Z(\phi) = \nabla_x \Theta(X^\Gamma(\phi)). \tag{14}$$

In general, the phase function $\Theta(x)$ is difficult to calculate, but the Z function is simple to compute and we will review some methods found in the literature [5, 12, 13].

4.2 The Adjoint method

In this section we will study the main method for computing the infinitesimal PRC, known as the Adjoint method. By linearizing our system around the periodic orbit, we can find a relation between the Adjoint of the linearized system and the iPRC that we will discuss in detail below.

Let $X^\Gamma(t) \in \Gamma$ be a T-periodic orbit of the system (13), and $y_0 \in \mathbb{R}^n$ an infinitesimal and arbitrary perturbation of the periodic orbit at time $t = 0$. Let $X(t)$ be the trajectory evolving from this perturbed initial condition. Defining $y(t)$ via $X(t) = X^\Gamma(t) + y(t)$, we have:

$$\dot{y} = A(t)y + O(|y|^2), \tag{15}$$

where $A(t) = DF|_{X^\Gamma(t)}$ and $y(0) = y_0$. Neglecting the smaller terms, solutions of the linearized equation satisfy:

$$(Ly)(t) := \dot{y} - A(t)y = 0. \tag{16}$$

We are interested in the Adjoint of the operator L.

Definition 4.4. *If $L : V \to U$ (V, U Hilbert spaces) is a linear operator, then the* **Adjoint linear operator**, *$L^* : U \to V$, satisfies $(u, Lv) = (L^*u, v)$ for all $u \in U$, $v \in V$, where $(\cdot, \cdot)$ is the standard inner product on T-periodic functions on $\mathbb{R}^n$:*

$$(u(t), v(t)) = \int_0^T u(t) \cdot v(t)dt.$$

The Adjoint L^* can be deduced easily:

$$\begin{aligned}
(u(t), Lv(t)) &= \int_0^T u(t) \cdot \left(\frac{d}{dt}v(t) - A(t)v(t)\right) dt \\
&= \int_0^T u(t) \cdot \frac{d}{dt}v(t)dt - \int_0^T u(t) \cdot A(t)v(t))dt \\
&= u(T) \cdot v(T) - u(0) \cdot v(0) - \int_0^T \frac{d}{dt}u(t) \cdot v(t)dt - \int_0^T A^T(t)u(t) \cdot v(t))dt \\
&= \int_0^T \left(-\frac{d}{dt}u(t) - A^T(t)u(t)\right) \cdot v(t)dt = (L^*u(t), v(t))
\end{aligned}$$

With this result, we define the Adjoint equation of (15) as:

$$\dot{z} = -A^T(t)z. \tag{17}$$

The Adjoint equation is very useful to us because the Z function defined in (14) is a solution. A simple proof can be seen in Brown et al. [14]. Recall that the PRC measures the phase shift and it is related to the Z function such that, in first order, $\Delta(\phi) = \Theta(X(t)) - \Theta(X^\Gamma(t)) = Z(\phi) \cdot y(t)$. By definition, the phase shift $\Delta(\phi)$ is independent of time. Therefore, using so and equation (16) we have:

$$
\begin{aligned}
0 &= \frac{d}{dt} Z(\phi) \cdot y, \\
&= \frac{dZ(\phi)}{dt} \cdot y + Z(\phi) \cdot \frac{dy}{dt}, \\
&= \frac{dZ(\phi)}{dt} \cdot y + Z(\phi) \cdot A(t) y, \\
&= \frac{dZ(\phi)}{dt} \cdot y + A(t)^T Z(\phi) \cdot y, \\
&= \left[\frac{dZ(\phi)}{dt} + A(t)^T Z(\phi) \right] \cdot y.
\end{aligned}
$$

Since the last term is true for any arbitrary perturbation near the limit cycle, we have that:

$$
-\frac{dZ(\phi)}{dt} - A(t)^T Z(\phi) = L^* Z = 0.
$$

Therefore, $Z(\phi)$ is a solution of the Adjoint equation. It remains to prove that it is unique.

First notice that if $X^\Gamma(t)$ is a T-periodic solution of the initial system (13), $X^\Gamma(t + t_0)$ is also a T-periodic solution for any $t_0 \in \mathbb{R}$. Also, we can see that $\frac{d}{dt} X^\Gamma(t)$ is a solution of $(Ly)(t) = 0$:

$$
\frac{d}{dt} \left(\frac{d}{dt} X^\Gamma(t) \right) = \frac{d}{dt} F(X^\Gamma(t)) = DF(X^\Gamma(t)) \frac{d}{dt} X^\Gamma(t) = A(t) \frac{d}{dt} X^\Gamma(t).
$$

Following this two facts and assuming that $X^\Gamma(t)$ is a stable periodic orbit, we can say that L has a nullspace of dimension 1 on the space of the T-periodic functions spanned by $\frac{d}{dt} X^\Gamma(t + t_0)$. It follows that the Adjoint operator L^* has a one-dimensional nullspace spanned by a T-periodic function. It is a consequence from Floquet theory that the Floquet multipliers of L (denoted by μ_i) and the Floquet multipliers of L^* (denoted by μ_i^*), are multiplicative inverses, $\mu_i \mu_i^* = 1$, for all i. Since a periodic solution has a Floquet multiplier 1 and there is only one periodic solution for L, there is also precisely one periodic solution for the Adjoint operator L^*. It remains to determine a proper normalization.

Using that $Z(t)$ is a solution of the Adjoint, we have that:

$$
\frac{d}{dt} (Z \cdot \frac{d}{dt} X^\Gamma(\phi)) = -A^T Z \cdot \frac{d}{dt} X^\Gamma(\phi) + Z \cdot A \frac{d}{dt} X^\Gamma(\phi) = 0
$$

Showing that Z must be proportional to $\frac{d}{dt} X^\Gamma$. The appropriate normalization follows from the observation that $\Theta(X^\Gamma(\phi)) = \phi$. Differentiating with respect to ϕ we get :

$$
Z(\phi) \cdot \frac{d}{d\phi} X^\Gamma(\phi) = 1, \tag{18}
$$

This condition uniquely defines $Z(t)$ as a solution of $L^* Z = 0$. This solution can be found numerically and methods will be explored in section 4.3.

4.3 Numerical methods to compute the PRC

In the previous section we have shown the relation between the PRC and the Adjoint equation. Next, we will apply numerical methods to find the solution of the Adjoint equation. The following methods are applied using the Morris-Lecar model (2) with the parameters given in (4).

The fist step is to compute numerically the periodic orbit Γ.

4.3.1 Finding periodic orbits using Poincaré sections

This method allows us to find a periodic orbit for a 2-dimensional system. Assume that we know, through a previous visualization (Figure 13) of the dynamics that there exists at least a periodic orbit and we know a Poincaré section which is transversal to the orbit. Let us define this section by the explicit equation $P(X) = 0$.

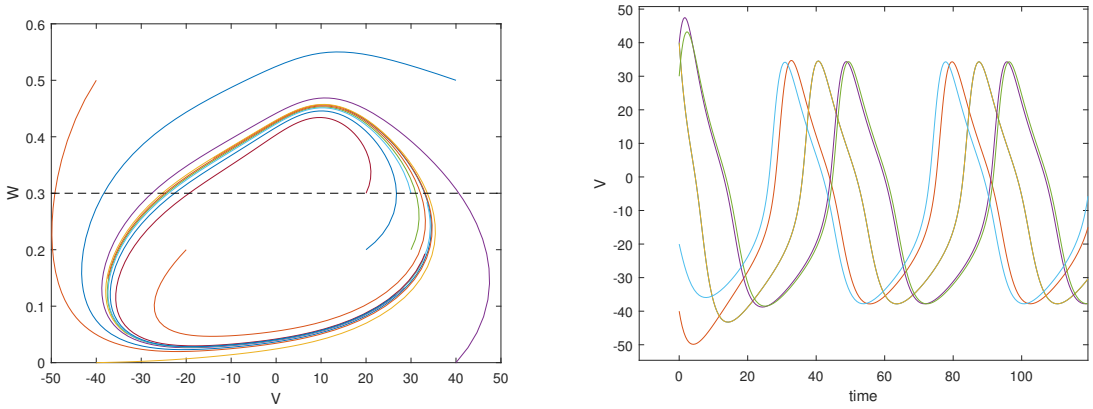

Figure 13: Dynamics of the Morris-Lecar model on the (V, w)-plane. There exists a stable periodic orbit. The black dashed line represents the Poincaré section chosen for the method $P(V, w) = w - 0.3 = 0$.

We define the Poincaré map $M(X(t_0))$ of a point $X(t_0)$ such that $P(X(t_0)) = 0$ ($X(t_0)$ belongs to the Poincaré section) as the point where the orbit $X(t)$, starting at $t = t_0$, crosses two times the Poincaré section $P(X) = 0$. Then $M(X(t_0)) = X(t_0 + T)$ where T is the time elapsed until the second crossing. Therefore, if we have $X(t_0)$ such that $M(X(t_0)) - X(t_0) = 0$, $X(t)$ corresponds to a T-periodic orbit. The method performs a bisection method on the Poincaré section until finding the point that remains invariant after crossing the section two times:

1. Select a Poincaré section $P(X) = 0$.

2. Find two initial points on the Poincaré section X_i^{in}, X_i^{out}, located inside and outside the orbit respectively. Calculate the middle point X_i between them.

3. Let us denote $X(t; X_i)$ as the solution of the system (2) with initial condition X_i. Use a Runge-Kutta method (or another numerical solver) to compute $X(t; X_i)$ until it crosses the Poincaré section for the second time.

4. Use the Newton's method on the integration time to calculate the time T_i and point of crossing $\hat{X}_i$ with the desired precision. Let $G(t_m) = P(X(t_m; X_i))$. The iteration scheme would be:

$$t_{m+1} = t_m - G(t_m)/G'(t_m),$$

until $|G(t_m)| < \epsilon$. Then we set $T_i = t_m$ and $\hat{X}_i = X(T_i; X_i)$

5. If $|\hat{X}_i - X_i|$ is greater than our desired tolerance, do $X_{i+1}^{in/out} = X_i$ depending on which side is X_i, calculate the middle point X_{i+1} and return to step 3.

6. If $|\hat{X}_i - X_i|$ is less than the desired tolerance, we have a point X_i that belongs to the periodic orbit and has period T_i.

An example of implementation of the method in MATLAB can be found in appendix D.

Using this method we can find the limit cycle for the Morris-Lecar model with the parameters given in (4) (See Figure 14).

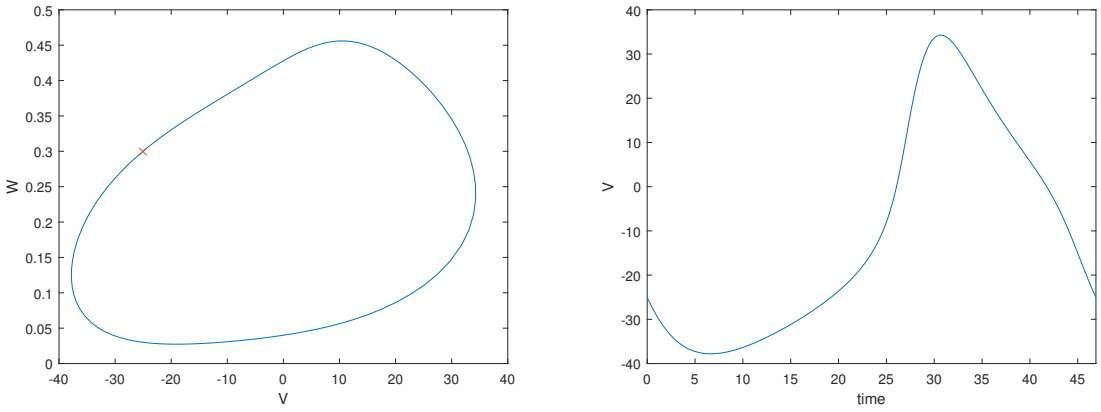

Figure 14: On the left, periodic orbit for the ML model on the $V - w$-plane found by integrating from the point $V = -25.050458314$, $w = 0.3$. The phase spans counterclockwise with a period of $T = 46.9$ms. On the right, time course of the V variable on the periodic orbit.

4.3.2 First method for computing the PRC: Poincaré sections.

In section 4.2 we have shown that the iPRC (Z function) is a periodic solution of the Adjoint linearized problem

$$\dot{z} = -A^T(t)z.$$

where $A = DF(X^\Gamma(t))$. Since A depends on the solution of the system (13) on time, one should solve this differential equation at the same time as equation (13), forming a 4-dimensional system (V, w, Z_1, Z_2). But we already have $X^\Gamma(t)$ from the previous section, so in practice we just have to find a periodic solution $(Z_1(t), Z_2(t))$ of the Adjoint equation (17). Thus, we can use the previous method again. We just need to find a suitable Poincaré section and two initial seeds. Recall the condition of the Adjoint (18):

$$Z(\phi) \cdot \frac{d}{d\phi} X^{\Gamma}(\phi) = 1 \implies G(Z) = Z_1(0)F_1(X^{\Gamma}(0)) + Z_2(0)F_2(X^{\Gamma}(0)) - 1 = 0.$$

We can use this condition as our Poincaré section. It just remains to find two points on the section that contain the solution in between them, we can do that visualizing some solutions along the section (see Figure 15). We choose $Z_1^{in} = -0.039$ and $Z_1^{out} = -0.0375$ and finally compute the Z function with the Poincaré method described in section 4.3.1 (Figure 16).

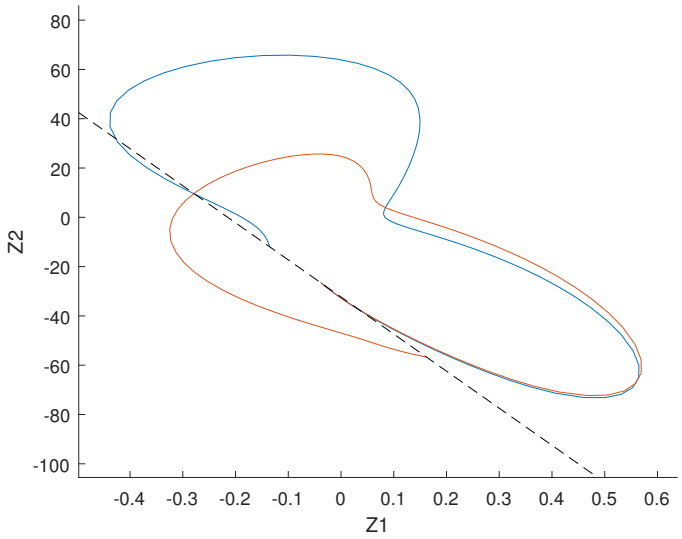

Figure 15: Poincaré section used to compute the PRC and initial points chosen. We show trajectories until they cross the Poincaré section for the second time: $Z_1^{in} = -0.039$ (blue) and $Z_1^{out} = -0.0375$ (red)

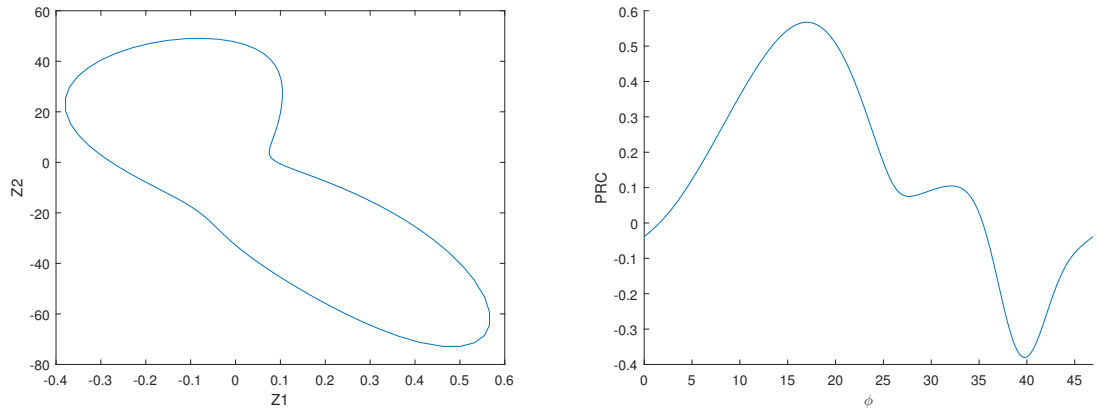

Figure 16: Z function computed for the Morris-Lecar model. Z function on the (Z_1, Z_2)-phase space (left) and the time course of the coordinate Z_1 which corresponds to the iPRC (right).

4.3.3 Second method for computing the PRC: Variational equations of the Adjoint

The first method relies heavily on numerical computations by just blindly trying to find periodic orbits and not really trying to find how should it be the solution of the Adjoint.

We recall that the fundamental matrix of a system of a homogeneous linear ordinary differential equations is a matrix-valued function $\Psi(t)$ whose columns are linearly independent solutions of the system. Then every solution to the system can be written as $x(t) = \Psi(t)c$, for some constant vector c. We can find the fundamental matrix by integrating the variational equations. So, we solve the system:

$$\begin{cases} \frac{d}{dt}\Psi(t) = -A^T(X^\Gamma(t))\Psi(t), \\ \Psi(t)|_{t=0} = Id. \end{cases} \tag{19}$$

In order to solve (19) for $\Psi(t)$ we need to compute the limit cycle $X^\Gamma(t)$ for $t \in (0, T)$, so integrate the original system (13) with an initial condition on the periodic orbit. This gives a system of $n + n \times n$ equations.

Then a solution $\bar{z}(t)$ of the Adjoint equation (17) satisfies $\bar{z}(t) = \Psi(t)c$, for c a constant vector. It remains to determine c . We know from section 4.2 that the Z function is unique T-periodic solution except for a constant. If we choose $c = v_1$, where v_1 is the eigenvector of $\Psi(T)$ with eigenvalue equal to one, we have:

$$\bar{z}(t+T) = \Psi(t+T)v_1 = \Psi(t)\Psi(T)v_1 = \Psi(t)v_1 = \bar{z}(t)$$

Therefore, $\bar{z}$ is a T periodic solution. Finally we define $z(t) = K\Psi(t)v_1$ and we choose K such that $z(t)$ satisfies the condition (18).

Proposition 4.1. *Let $X^\Gamma(t)$ be a T-periodic limit cycle of (13), $\Psi(t)$ the fundamental matrix of the Adjoint linear system (17) and v_1 the eigenvector of eigenvalue equal to 1 of $\Psi(T)$. Then:*

$$Z(t) = \frac{\Psi(t)v_1}{\langle \Psi(t)v_1, F(X^\Gamma(t))\rangle}, \tag{20}$$

is a T-periodic solution of the Adjoint linear system that satisfies the condition (18), i.e. is the Z function .

We can use this proposition to design an algorithm, which consists on the following steps:

1. Find a limit cycle of the initial system (13) $X^\Gamma(t)$ and a period T using the Poincaré section method explained in section 4.3.1.
2. Use a point from the limit cycle as initial point to integrate the $n + n \times n$ variational equations (19) a time T, getting the fundamental matrix $\Psi(T)$
3. Find the eigenvectors of $\Psi(T)$ and save v_1 as the eigenvector of eigenvalue 1.
4. Discretize $[0, T)$ in k points and find the solution of the variational equations $\Psi_i := \Psi(i\frac{T}{k})$ $(i = 1...k)$ and $X_i^\Gamma := X^\Gamma(i\frac{T}{k})$ as in step 2.
5. Compute $Z_i = \Psi_i v_1 / \langle \Psi_i v_1, F(X_i^\Gamma)\rangle$

Figure 17 shows the results of applying this method to the Morris-Lecar model.

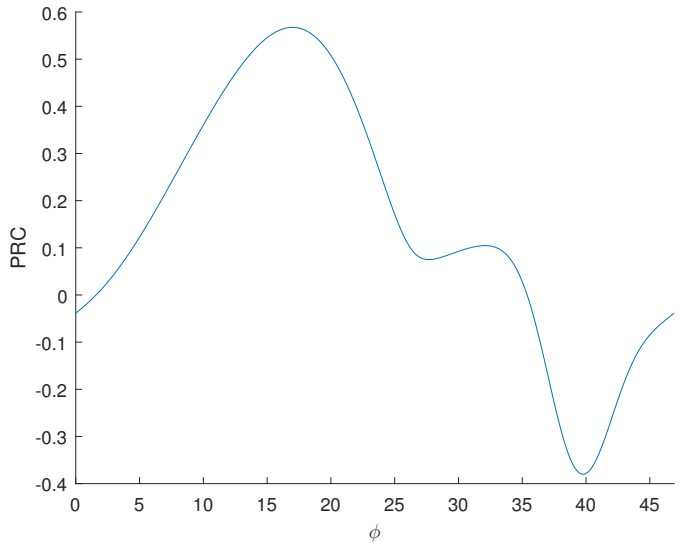

Figure 17: First component of the Z function (voltage) computed for the Morris-Lecar model using the method described in section 4.3.3.

4.3.4 Third method for computing the PRC: Variational equations of the initial system

In Guillamon-Huguet (2008) [12] a solution of the Adjoint is found as a function of the fundamental matrix of system (15) instead of the Adjoint. There, we find the proof for the following proposition:

Proposition 4.2. *Let Γ be a T-periodic orbit of a planar analytic vector field F as in (13) . Then, the Adjoint equation (17) and the condition (18) is satisfied by $Q(t)$ defined as:*

$$Q(t) = \frac{JK(t)}{\langle JK(t), F(X^{\Gamma}(t))\rangle} \tag{21}$$

with

$$K(t) = e^{\lambda \frac{t}{T}} \Psi(t) v_2, \qquad J = \begin{bmatrix} 0 & -1 \\ 1 & 0 \end{bmatrix},$$

where $\Psi(t)$ is the solution of the variational equations on the original linear system (16), λ is the eigenvalue of $\Psi(T)$ such that $\lambda < 1$ and v_2 its eigenvector.

An example of implementation of the method in MATLAB can be found in appendix D.

4.3.5 Similarities between the methods

The second and third method share the same main idea, using the variational equations of the system or the Adjoint equation in order to find the solution. The first method relies on finding the solution on a section by computing the Poincaré map several times, which requires higher numerical precision if the periodic orbit we are trying to find is unstable, and this is exactly the case. The Poincaré method works well for

finding the periodic orbit on the initial system since it is stable. However, the periodic orbit of the Adjoint is unstable and requires higher numerical precision, so we will use the other methods to compute it. All computations have been done with either the second or third methods with similar results and computing costs, so they can be used without distinction.

4.4 The relation between the PRC and the response to inputs

The phase-resetting curve (PRC) describes the response of an oscillator to a single pulse, but it can also be used to study its response to a periodic pulse train, as seen in Izhikevich [15]. Let us denote by ϕ_n the phase of oscillation at the time the n-th input pulse arrives. Such a pulse resets the phase by $PRC(\phi_n)$, so that the new phase right after the pulse is $\phi_n + \mathrm{PRC}(\phi_n)$. Let T_s denote the period of pulsed stimulation. Then the phase of oscillation before the next, $(n+1)$-th, pulse is $\phi_n + PRC(\phi_n) + T_s$. Thus, we have a mapping for the subsequent values of the phase (See Figure 18).

Definition 4.5. *The map $\mathcal{F} : [0, T) \to [0, T)$ given by*

$$\phi_{n+1} = \mathcal{F}(\phi_n) = \phi_n + PRC(\phi_n) + T_s \quad mod\ T \tag{22}$$

is called the Poincaré phase map.

Definition 4.6. *The sequence $\{\phi_n\}_{n\in\mathbb{N}}$ is called the orbit of the Poincaré phase map.*

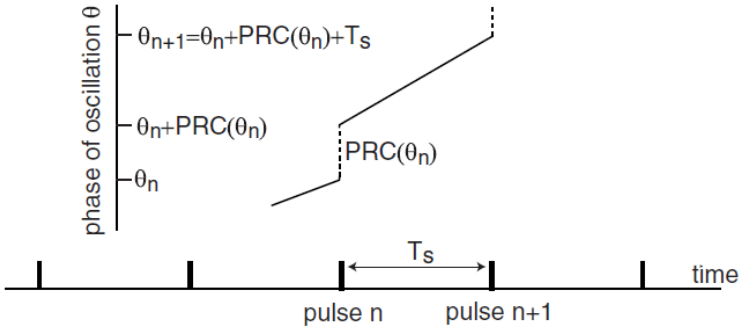

Figure 18: Calculations of the Poincaré Phase Map. Image from Izhikevich [15]

4.4.1 Synchronization to an external stimulus

The dynamics of the Poincaré phase map will show us the behaviour of an oscillator being periodically stimulated. A fixed point of the map (22) satisfies that:

$$\phi + T = \phi + \mathrm{PRC}(\phi) + T_s \quad \Longrightarrow \quad \mathrm{PRC}(\phi) = T - T_s.$$

The last expression corresponds to the intersection of the PRC with the horizontal line $T - T_s$ as shown in Figure 19. We can see that for large positive and negative values of $T - T_s$ a fixed point of the map does not exist, and it is only possible when it is between the maximum and minimum of the PRC. When $T - T_s$ is between those values, synchronization occurs with a phase shift θ, depending on the position of the intersection.

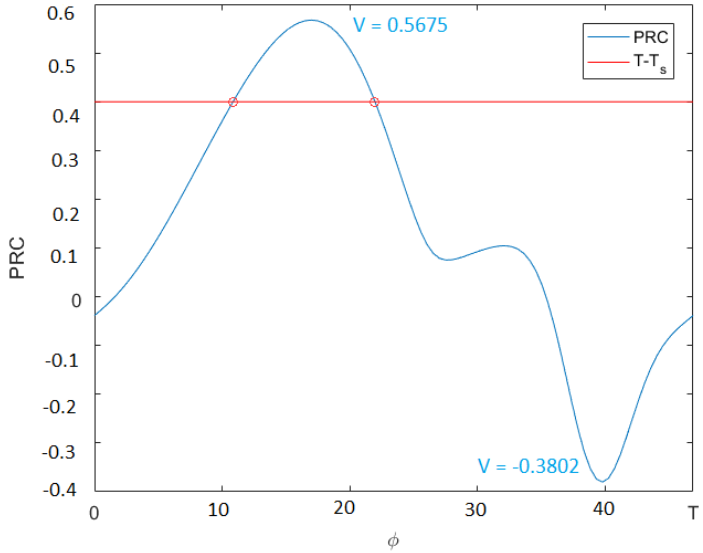

Figure 19: Fixed points of the Poincaré phase map for the PRC of the ML model, for a perturbation in the direction $(V, w) = (1, 0)$ and period T_s. Values of maximum and minimum are indicated in blue.

In order to check the stability of the fixed points, we recall that if ϕ^* is a fixed point of $\mathcal{F}(\phi)$:

- If $|\mathcal{F}'(\phi^*)| < 1$, the fixed point is **stable**.
- If $|\mathcal{F}'(\phi^*)| > 1$, the fixed point is **unstable**.

Therefore, if $\mathcal{F}(\phi) = \phi + \text{PRC}(\phi) + T_s$ we can find a region of stability:

$$\begin{aligned} |\mathcal{F}'(\phi)| = |1 + \text{PRC}'(\phi)| &< 1, \\ -1 < 1 + \text{PRC}'(\phi) &< 1, \\ -2 < \text{PRC}'(\phi) &< 0. \end{aligned}$$

For a periodic perturbation of 1 mV in the direction of the voltage and period T_s we can approximate the PRC of the ML model as the first component of the infinitesimal PRC:

$$PRC(\phi) = Z(\phi) \cdot y = Z(\phi) \cdot \begin{bmatrix} 1 \\ 0 \end{bmatrix} = Z_V(\phi).$$

Then, the ML model can only synchronize for perturbations of period $0.5675 \geq T_s \geq -0.3802$. When T_s is within these values, we wil always have two equilibrium points, one stable and one unstable (Figure 20), until they coalesce at a saddle-node bifurcation (more about bifurcations on Appendix A).

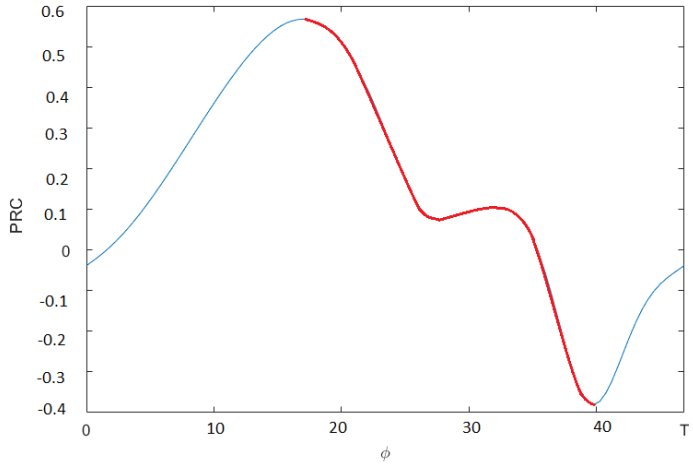

Figure 20: Stability of the fixed points of the Poincaré phase map for the ML model with a perturbation of $V = 1$. In red, regions of stability, in blue: regions of instability. There is a saddle at the intersection of the regions.

4.5 Weak Coupling with identical oscillators

Our ultimate goal is to study the synchronization of oscillators. Until now all models were about a single oscillator. The next step is to add another one, with the same or similar dynamics, and a way to couple them. Models for coupled neurons are widely studied and coupling is often formulated as an ionic-channel-like conductance as described in (5). However, the basic premise of PRC theory is that the stimulus is **weak** so that it might affect the phase but it does not affect the shape of the orbit. In order to do that, we will consider $\bar{g}$ in equation (5) such that the coupling is weak.

The general formulation consists in considering two identical oscillators that are coupled to each other with a coupling function multiplied by a constant ϵ:

$$\begin{aligned} \frac{dX_1}{dt} &= F(X_1) + \epsilon G_1(X_1, X_2), \\ \frac{dX_2}{dt} &= F(X_2) + \epsilon G_2(X_2, X_1). \end{aligned} \tag{23}$$

Consider the phase variable $\phi_i = \Theta(X_i)$ where Θ is the asymptotic phase function defined in section 4.1, differentiating we get:

$$\begin{aligned} \frac{d}{dt}\phi_i &= \frac{d}{dt}\Theta(X_i) \\ &= \nabla_x \Theta(X_i) \cdot \frac{dX_i}{dt} + \epsilon \nabla_x \Theta(X_i) \cdot G_i(X_i, X_j), \\ &= 1 + \epsilon \nabla_x \Theta(X_i) \cdot G_i(X_i, X_j), \end{aligned}$$

for $i, j = 1, 2$, $i \neq j$. The last equality follows from equation (18). Indeed, since ϵ is small, $X_i(t)$ is close to the limit cycle $X^\Gamma(t)$. Therefore, system (23) becomes an equation involving only the phases of the

oscillators:

$$\frac{d\phi_1}{dt} = 1 + \epsilon \nabla_x \Theta(X^\Gamma(\phi_1)) \cdot G_1(X^\Gamma(\phi_1), X^\Gamma(\phi_2)), \tag{24}$$

$$\frac{d\phi_2}{dt} = 1 + \epsilon \nabla_x \Theta(X^\Gamma(\phi_2)) \cdot G_2(X^\Gamma(\phi_2), X^\Gamma(\phi_1)). \tag{25}$$

First, we introduce the change of variables $\theta_j = \phi_j - t$ and we obtain:

$$\frac{d\theta_i}{dt} = \epsilon \nabla_x \Theta(X^\Gamma(t + \theta_i)) \cdot G_i(X^\Gamma(t + \theta_i), X^\Gamma(t + \theta_j)). \tag{26}$$

Note that equation (26) has the form:

$$y' = \epsilon M(y, t)$$

where M is T-periodic in time. Expressions of this kind, with an oscillatory dynamics but slowed down by the term ϵ can be **averaged**. There is more information about the averaging theory in Appendix B. The averaging theorem ensures us that y will be close to its average $\bar{y}$, where the dynamics for $\bar{y}$ is described by the equation n

$$\bar{y}' = \epsilon \frac{1}{T} \int_0^T M(\bar{y}, t) dt.$$

In order to simplify the exposition, we will abuse notation denoting $y := \bar{y}$, or in the case of equation (26), $\theta_i := \bar{\theta}_i$. Applying the averaging theory to equation (26) results in the following equations:

$$\begin{aligned} \frac{d\theta_1}{dt} &= \epsilon H_1(\theta_2 - \theta_1), \\ \frac{d\theta_2}{dt} &= \epsilon H_2(\theta_1 - \theta_2), \end{aligned} \tag{27}$$

where

$$H_j(\theta) = \frac{1}{T} \int_0^T Z(t) \cdot G_j[X^\Gamma(t), X^\Gamma(t + \theta)] dt, \tag{28}$$

and the function H is called the **interaction function.**

The Z function (iPRC), G_j (the coupling functions) and Γ (the limit cycle) are all known, so it is possible to simply calculate the integral H, probably with numerical integration, and study stability directly on (27). Notice though that the variables on the left hand side appear only as the difference between them, and that equals the difference of phases: $\theta_2 - \theta_1 = \phi_2 - t - \phi_1 + t = \phi_2 - \phi_1$. Subtracting the two equations of (27) and using the change of variables $\psi = \theta_2 - \theta_1$ results on the following 1 dimensional equation that stands for the phase difference:

$$\frac{d\psi}{dt} = \epsilon[H_2(-\psi) - H_1(\psi)]. \tag{29}$$

Moreover, if the oscillators were coupled with the same coupling function, i.e. $G_1(X_1, X_2) = G_2(X_1, X_2) = G(X_1, X_2)$ we will have just -2 times the odd function ($f^{odd}(x) = [f(x) - f(-x)]/2$) of H.

$$\frac{d\psi}{dt} = -2\epsilon H^{odd}(\psi). \tag{30}$$

Notice that (29) and (30) are 1-dimensional ODEs, which are easy to study. Studying the dynamics of this system will tell us relevant information about the synchronization of the oscillators. More precisely,

- Equilibrium points $\psi = c$ correspond to states where the difference of phases is constant equal to c, meaning that the oscillators evolve at the same speed frequency, but separated by a fixed time, synchronized **out-of-phase**.
- If $\psi = 0$ is a stable equilibrium point, the oscillators will synchronize **in-phase**.
- If $\psi = \frac{1}{2}$ is a stable equilibrium point, the oscillators will synchronize in **anti-phase**.

4.5.1 Synchronization of two identical neurons using the ML model

We will apply the method described in section 4.5 to study synchronization properties of two mutually coupled identical neurons, modeled by the Morris-Lecar model as described in equation (5).

We assume $\bar{g}$ ($\bar{g} = \epsilon$) small, $n = 2$, therefore:

$$G_1\left[(V_1, w_1, s_1), (V_2, w_2, s_2)\right] = [-s_2(V_1 - V_{syn}), 0, 0],$$

$$G_2\left[(V_2, w_2, s_2), (V_1, w_1, s_1)\right] = [-s_1(V_2 - V_{syn}), 0, 0].$$

We will study two cases, inhibitory ($V_{syn} = -75$) and excitatory ($V_{syn} = 120$). For the method, we just need to compute H:

$$H(\phi) = \frac{1}{T}\int_0^T Z(t) \cdot G[X^\Gamma(t), X^\Gamma(t+\phi)]dt.$$

The numerical computations performed can be summarized as:

1. Numerically find $X^\Gamma(t)$ and T, using the Poincaré section method described in section 4.3.1.
2. Numerically find the Z function, using one of the methods previously described in section 4.3, e.g. the Adjoint method described in section 4.3.3.
3. Solve the integral with a numerical method. If we obtained Z using the Adjoint equation, we have its value for ϕ_i in equally separated intervals. We can then use a Newton-Cotes method such as Simpson's rule or higher order ones. For this case, Boole's 4/90 Rule was used.

Figure 21 shows the H and $-H^{odd}$ functions for the inhibitory case and Figure 22 for the excitatory case.

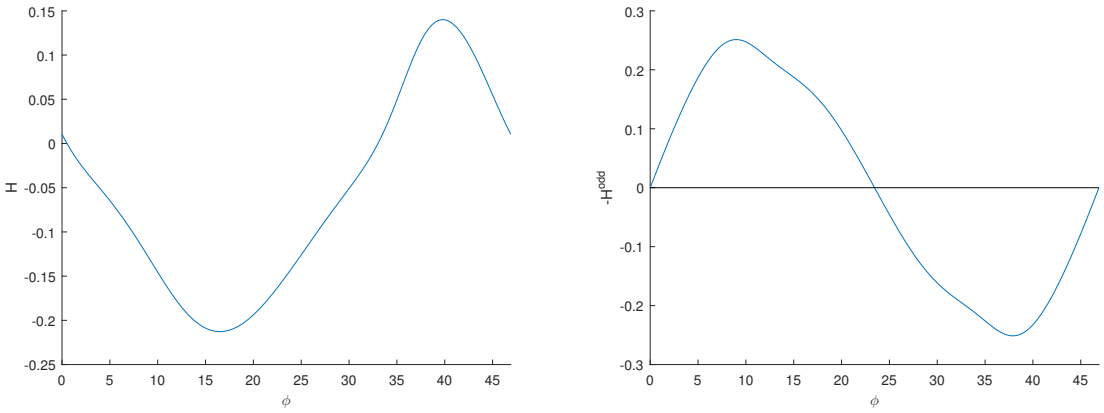

Figure 21: Inhibitory case of the ML model for two coupled neurons: On the left the resulting interaction function H found by the numerical integration. On the right, $-H_{odd}$.

We can study the dynamics of the phase difference using the computed value of H in Figure 21. The phase equation has two fixed points where $-H_{odd}$ vanishes (recall that point at $\phi = 0$ is identified with the one at $\phi = T$). The fixed point on $\phi = 0$ is unstable and the one at $\phi = T/2$ is stable, thus neurons with inhibitory connections tend to synchronize in anti-phase.

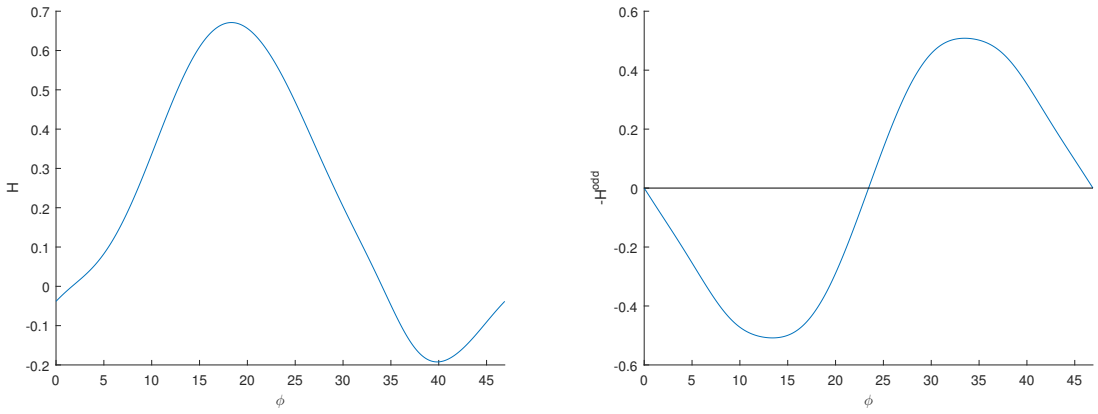

Figure 22: Excitatory case of the ML model for two coupled neurons: On the left the resulting interaction function H found by the numerical integration. On the right, $-H_{odd}$.

In the excitatory case there exist also two fixed points, but now the fixed point on $\phi = 0$ is stable and the one at $\phi = T/2$ is unstable, thus they tend to synchronize in phase.

4.6 Weak coupling with non identical oscillators

Consider two different small deviations of order ϵ on each oscillator in order to make them not identical but still similar, that is,

$$\begin{aligned} \frac{dX_1}{dt} &= F(X_1) + \epsilon f_1(X_1) + \epsilon G_1(X_1, X_2), \\ \frac{dX_2}{dt} &= F(X_2) + \epsilon f_2(X_2) + \epsilon G_2(X_2, X_1). \end{aligned} \tag{31}$$

Therefore,

$$\begin{aligned} \frac{d\phi_1}{dt} &= 1 + \epsilon f_1(X^\Gamma(\phi_1)) + \epsilon \nabla_x \Theta_1(X^\Gamma(\phi_1)) \cdot G_1(X^\Gamma(\phi_1), X^\Gamma(\phi_2)), \\ \frac{d\phi_2}{dt} &= 1 + \epsilon f_2(X^\Gamma(\phi_2)) + \epsilon \nabla_x \Theta_2(X^\Gamma(\phi_2)) \cdot G_2(X^\Gamma(\phi_2), X^\Gamma(\phi_1)). \end{aligned} \tag{32}$$

$$\begin{aligned} \frac{d\theta_1}{dt} &= \epsilon \nabla_x \Theta(X^\Gamma(t+\theta_1)) \cdot \left[f_1(X^\Gamma(\theta_1)) + G(X^\Gamma(t+\theta_1), X^\Gamma(t+\theta_2)) \right], \\ \frac{d\theta_2}{dt} &= \epsilon \nabla_x \Theta(X^\Gamma(t+\theta_2)) \cdot \left[f_1(X^\Gamma(\theta_1)) + G_2(X^\Gamma(t+\theta_2), X^\Gamma(t+\theta_1)) \right]. \end{aligned} \tag{33}$$

Applying the averaging to (33) results in the following equations:

$$\begin{aligned} \frac{d\theta_1}{dt} &= \epsilon \bar{H}_1(\theta_2 - \theta_1), \\ \frac{d\theta_2}{dt} &= \epsilon \bar{H}_2(\theta_1 - \theta_2), \end{aligned} \tag{34}$$

where

$$H_i(\theta) = \frac{1}{T} \int_0^T Z(t) \cdot f_i[X^\Gamma(t)] dt + \frac{1}{T} \int_0^T Z(t) \cdot G_i[X^\Gamma(t), X^\Gamma(t+\theta)] dt. \tag{35}$$

We define:

$$\omega_i := \frac{1}{T} \int_0^T Z(t) \cdot f_i[X^\Gamma(t)] dt,$$

as a constant frequency deviation from the free-running oscillation. Therefore,

$$\begin{aligned} \frac{d\theta_1}{dt} &= \epsilon \omega_1 + \epsilon H_1(\theta_2 - \theta_1), \\ \frac{d\theta_2}{dt} &= \epsilon \omega_2 + \epsilon H_2(\theta_1 - \theta_2), \end{aligned} \tag{36}$$

with H defined as in (28).

Subtracting the two equations of (34) and using the change of variables $\psi = \theta_2 - \theta_1$ and $\Delta\omega = \omega_2 - \omega_1$ results in:

$$\frac{d\psi}{dt} = \epsilon[\Delta\omega + H_2(-\psi) - H_1(\psi)]. \tag{37}$$

This time a fixed point takes place when $H_2(-\psi) - H_1(\psi)$ intersects the horizontal line $\Delta\omega$.

4.6.1 Synchronization of two non-identical neurons using the ML model

If we assume that both neurons follow the same ML model (5), but with a slight difference on their periods, that the limit values are around $|\Delta\omega| < 0.5$ for the excitatory case (Figure 23) and $|\Delta\omega| < 0.25$ for the inhibitory (Figure 24); inside this range, two fixed points always exists. At the limits, a saddle-node bifurcation occurs, the two fixed points coalesce at one fixed point that is no longer hyperbolic, and disappears afterwards.

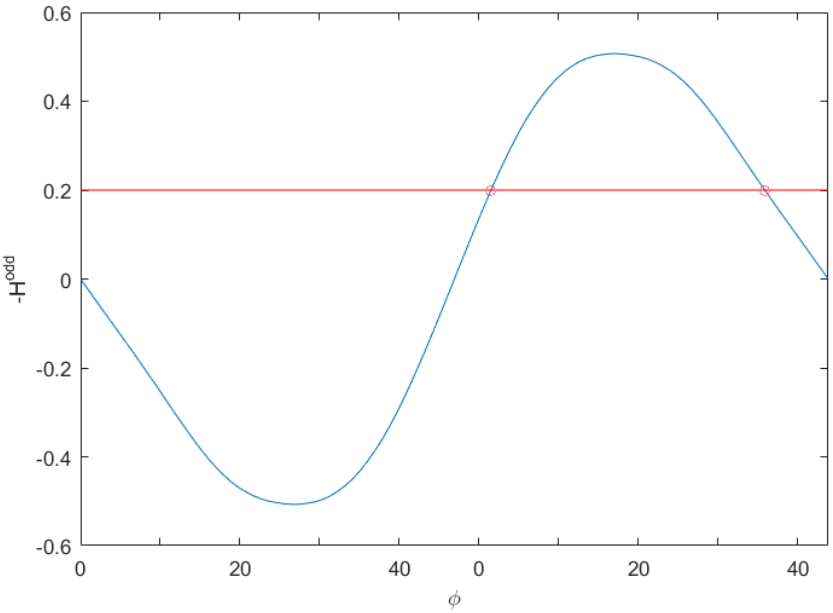

Figure 23: Excitatory case of the ML model for two non identical neurons, for $\Delta\omega = 0.2$.

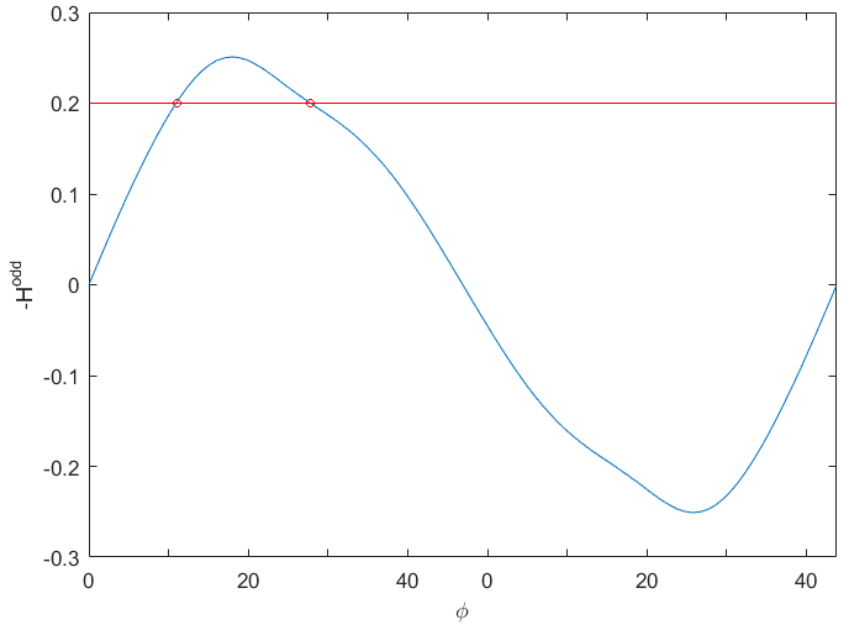

Figure 24: Inhibitory case of the ML model for two non identical neurons, for $\Delta\omega = 0.2$.

4.7 Weak coupling for 3 or more oscillators

We start with the usual assumptions, considering identical oscillators coupled between them with a coupling function G and a small coupling strength. We can choose between different coupling configurations:

- All-to-all coupling: All oscillators are coupled with the others both ways (Figure 25).
- Chain connection: Oscillators are displayed in a row and coupled with its nearest neighbour.
- Cycle connection: Same as before, but the first and the last oscillator are coupled. Same as fully connected for the case of 3 oscillators.
- Other types of connection with a certain topology.

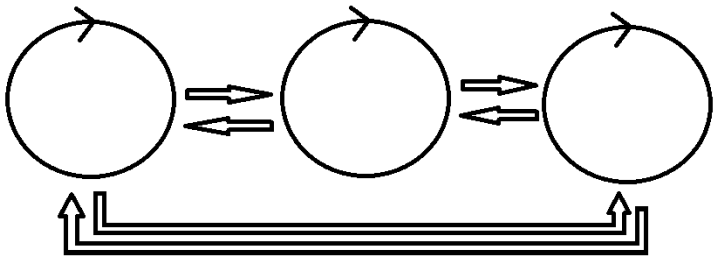

Figure 25: Diagram of 3 oscillators with all-to-all coupling.

For the case of $n = 3$ and all-to-all coupling the equations are:

$$\begin{aligned}\frac{dX_1}{dt} &= F(X_1) + \epsilon[G_1(X_1, X_2) + G_1(X_1, X_3)],\\ \frac{dX_2}{dt} &= F(X_2) + \epsilon[G_2(X_2, X_1) + G_2(X_2, X_3)],\\ \frac{dX_3}{dt} &= F(X_3) + \epsilon[G_3(X_3, X_1) + G_3(X_3, X_2)].\end{aligned} \tag{38}$$

We proceed the same way as in the two oscillator case and obtain:

$$\frac{d\phi_i}{dt} = \epsilon[\nabla_x \Theta(X^\Gamma(t+\phi_i)) \cdot G_i(X^\Gamma(t+\phi_i), X^\Gamma(t+\phi_j)) + \nabla_x \Theta(X^\Gamma(t+\phi_i)) \cdot G_i(X^\Gamma(t+\phi_i), X^\Gamma(t+\phi_k))], \tag{39}$$

$i, j, k = 1, 2, 3,\ i \neq j \neq k$.

$$\begin{aligned}\frac{d\phi_1}{dt} &= \epsilon[H(\phi_2 - \phi_1) + H(\phi_3 - \phi_1)],\\ \frac{d\phi_2}{dt} &= \epsilon[H(\phi_1 - \phi_2) + H(\phi_3 - \phi_2)],\\ \frac{d\phi_3}{dt} &= \epsilon[H(\phi_1 - \phi_3) + H(\phi_2 - \phi_3)].\end{aligned} \tag{40}$$

We define $\psi_1 = \theta_2 - \theta_1$, $\psi_2 = \theta_3 - \theta_2$. We define ψ_1 as the phase difference between the first and the second oscillator, and ψ_2 is the phase difference between the second and the third oscillator. Therefore,

$$\begin{aligned}\frac{d\psi_1}{dt} &= \epsilon[H(-\psi_1) + H(\psi_2) - H(\psi_1) - H(\psi_1 + \psi_2)],\\ \frac{d\psi_2}{dt} &= \epsilon[H(-\psi_2) - H(-\psi_1) - H(\psi_2) + H(-\psi_1 - \psi_2)].\end{aligned} \tag{41}$$

The last expression is the 3-oscillator version of (29). We identify the following synchronized states:

- If $\psi_1 = 0$, $\psi_2 = 0$ is a stable fixed point, the three oscillators will synchronize in-phase.
- If $\psi_1 = 0$, $\psi_2 = k$ is a stable fixed point, two oscillators will synchronize while the third will be out of phase with respect to the others.
- If $\psi_1 = 1/3$, $\psi_2 = 1/3$ or $\psi_1 = 2/3$, $\psi_2 = 2/3$, the oscillators will synchronize out of phase but at the same "temporal" distance from each other. This corresponds to the three oscillator version of being in anti-phase.
- A general configuration where $\psi_1 = d_1$, $\psi_2 = d_2$, the oscillators will synchronize out of phase and at the different distances from each other.

4.7.1 Synchronization of three neurons using the ML model

In this section we will apply the method described in section 4.7 to the Morris Lecar model (5) for $n = 3$ and the same coupling term. We already have $H(\psi)$ from section 4.5.1, so we use it to calculate the expression in (41).

We obtained $H(\psi)$ numerically and only on a finite number N of points. We take advantage of the fact that it is a T-periodic function and use a method of interpolation Fourier coefficients that will be computed using the **Fast Fourier Transform**. The method is described in Appendix C.

Figures 26 and 27 show the nullclines of a three neuron system, for the inhibitory and excitatory couplings respectively, computed by interpolating H using the FFT and calculating:

$$H(-\psi_1) + H(\psi_2) - H(\psi_1) - H(\psi_1 + \psi_2) = 0,$$
$$H(-\psi_2) - H(-\psi_1) - H(\psi_2) + H(-\psi_1 - \psi_2) = 0.$$

We can observe clearly from the plots the symmetry of the system (the nullclines presents a symmetry with respect to the axis $y = T - x$). This symmetry is a consequence of having three identical oscillators with identical coupling.

Using our interpolated H, we can compute the fixed points and also the Jacobian of the system (41) and its eigenvalues. We observe several equilibrium points corresponding to the intersection of the nullclines, which are given explicitly in tables 1 and 2 for inhibitory and excitatory coupling, respectively.

Notice that the equilibrium points of the inhibitory case have opposite stability of the ones for the excitatory case. Note also that the saddles that appear have inverted stable and unstable invariant manifolds.

Table 1: Fixed points on the 3 neurons inhibitory model. $T = 46.90071$

Point: (ψ_1, ψ_2)	Eigenvalues of the Jacobian	Type	Comments
(0, 0)	0.00888, 0.00888	Unstable node	The neurons will not synchornize in phase as expected from inhibitory coupling.
(T/3, T/3)	-0.00385+0.00310i, -0.00385-0.003102i	Stable focus	The neurons will synchronize out of phase but at the same "distance" from each other
(0, 19.75428)	0.00463, -0.00708	Saddle	Neurons 1 and 2 synchronize in phase, neuron 3 does not.
(T-19.75428, 0)	0.00463, -0.00708	Saddle	Neurons 2 and 3 synchronize in phase, neuron 1 does not.
(19.75428, T-19.75428)	0.00463, -0.00708	Saddle	Neurons 1 and 3 synchronize in phase, neuron 2 does not.

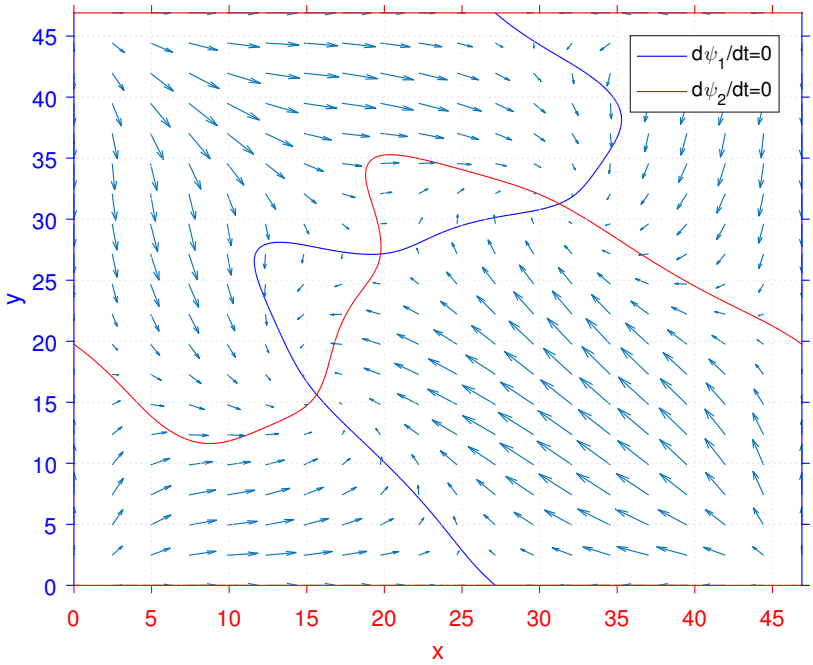

Figure 26: Nullclines of the ML system for three neurons with all-to-all inhibitory coupling. The intersections of the nullclines determine the equilibrium points.

Table 2: Fixed points on the 3 neurons excitatory model. $T = 46.90071$

Point: (ψ_1, ψ_2)	Eigenvalues of the Jacobian	Type	Comments
(0,0)	-0.01419, -0.01419	Stable node	The neurons will synchornize in phase as expected from excitatory coupling.
(T/3,T/3)	0.00669 + 0.01086i, 0.00669 - 0.01086i	Unstable focus	The neurons will not synchronize with the same phase difference between them.
(0, 19.04341)	-0.00865, 0.01801	Saddle	Neurons 1 and 2 synchronize in phase, neuron 3 does not.
(T-19.04341,0)	-0.00865, 0.01801	Saddle	Neurons 2 and 3 synchronize in phase, neuron 1 does not.
19.04341,T-19.04341)	-0.00865, 0.01801	Saddle	Neurons 1 and 3 synchronize in phase, neuron 2 does not.

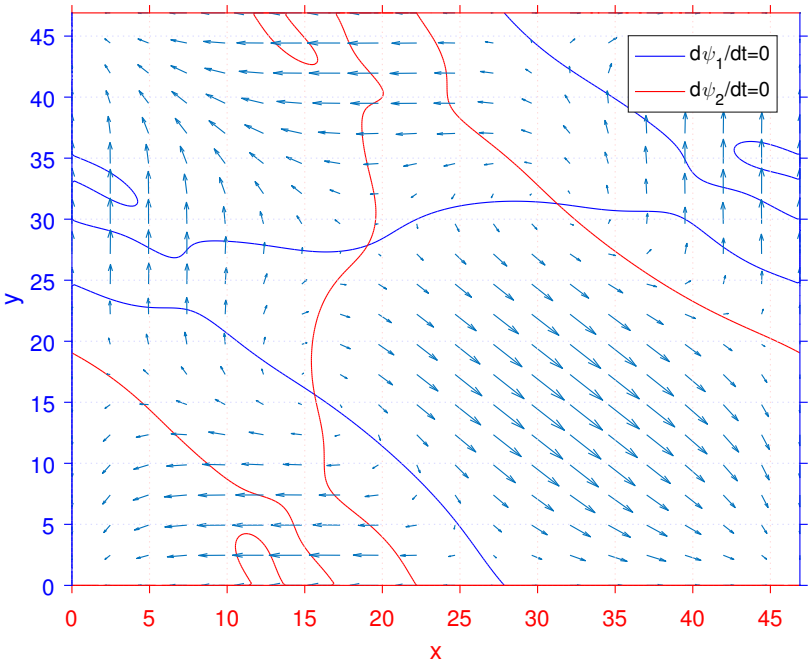

Figure 27: Nullclines of the ML system for three neurons with all-to-all excitatory coupling. The intersections of the nullclines determine the equilibrium points.

5 Memristor Devices

In the previous section, we performed the exploration of different concepts and procedures used in neuroscience to study perturbations of neuronal oscillation and synchronization properties. In this section, we will use these tools to provide a description of the synchronization properties for the models of memristic circuits described in section 3.2.

5.1 The Phase Resetting Curve on Menristor Devices

Consider the model (8) for the memristor circuit we defined on section 3.2 for the set of parameters given in (9) for which the voltage shows oscillations.

We compute the periodic orbit using Poincaré sections (See Figure 28). Note that the oscillation of the resistance is as expected, since its dynamics is faster than the voltage and almost only takes two values, $R_h = 100\Omega$ and $R_l = 10\Omega$. This quick transition is visible on the periodic orbit as sharp edges of the cycle (See Figure 28-right).

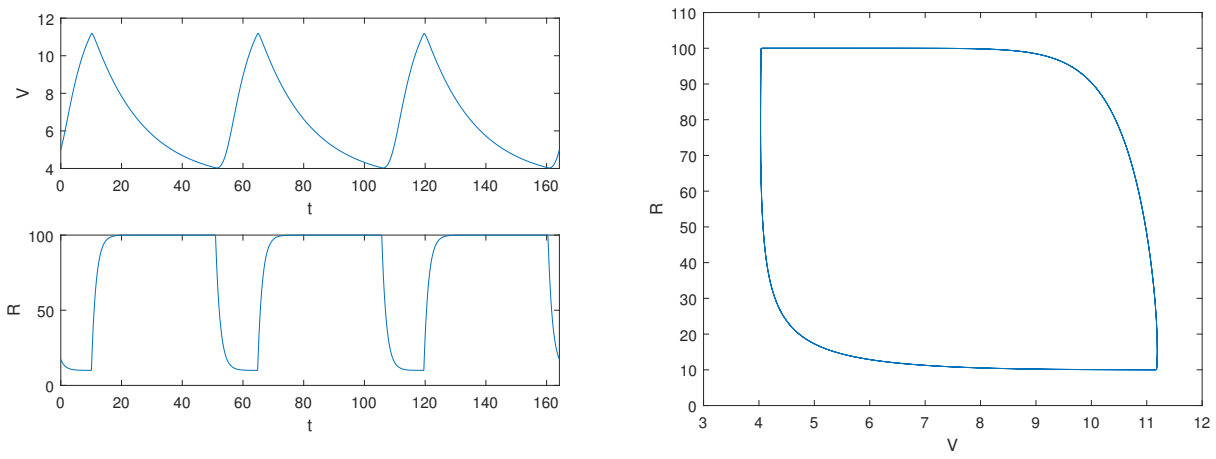

Figure 28: Left: Time course of the voltage and memristor resistance for the memristor circuit. Right: Stable limit cycle on the V-R plane for the system (8) and parameter values (9).

Figure 29 shows the PRC for the limit cycle obtained by computing the Z function using the method of variational equations described in section 4.3.4. The PRC provides information about the phase change due to a voltage perturbation at a given point on the periodic orbit. Notice that the PRC is 70% of the time negative. Moreover, we observe that the positive part of the PRC corresponds to the time when the resistance is low ($R = R_l$), while the negative part corresponds to the time when the resistance is high ($R = R_h$). A negative PRC indicates that an impulse at that point would delay the phase, so the memristor model is most of the time delayed rather than advanced.

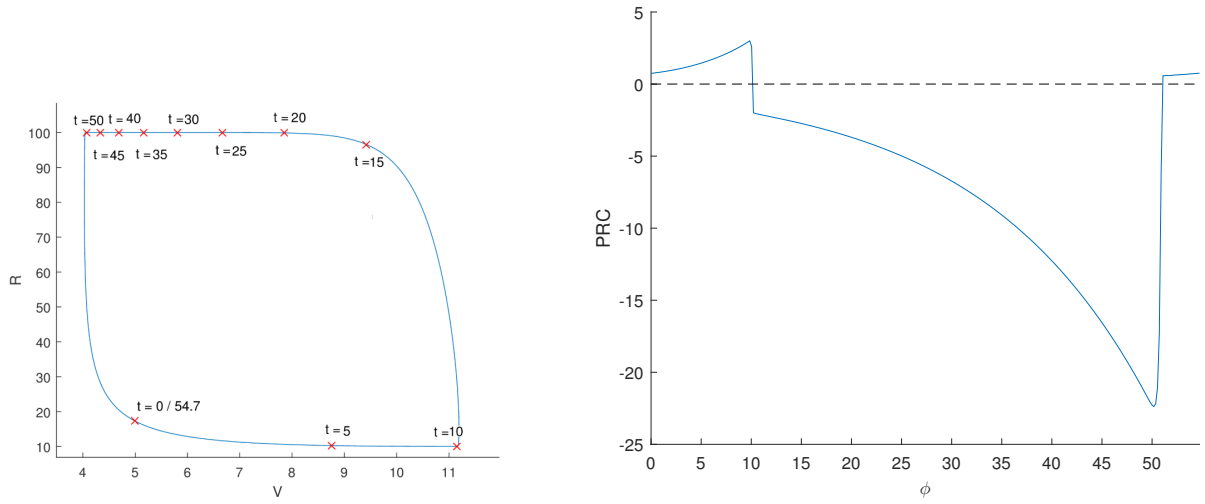

Figure 29: Left: Limit cycle on the V-R plane for the memristor circuit model with time labels for the oscillation. Right: Phase resetting curve of the memristor circuit model computed using the variatonal method (4.3.4).

5.1.1 Memristor synchronization to a periodic external stimulus

If we consider a periodic perturbation as in section 4.4.1, synchronization will be possible when the period of the perturbation is near the period of the memristor oscillation, and the limits for this difference are the maximum and minimum of the PRC. Figure 30 shows an example for which this condition is met, and the Poincaré phase map has two fixed points, indicating how has the memristor synchronized with the external periodic perturbation. The value ϕ_s of the fixed point, indicates that the synchronization is out-of-phase by a constant ϕ_s.

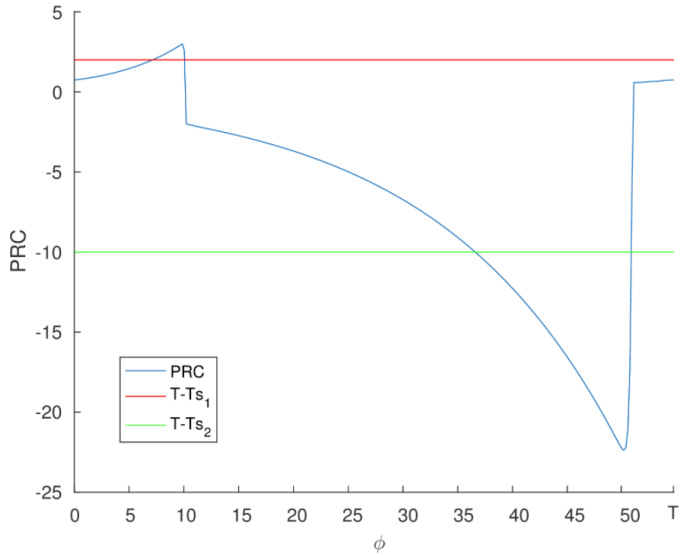

Figure 30: Poincaré phase map of the memristor model subject to two periodic stimulus of period S_1 and S_2. Intersections indicate fixed points.

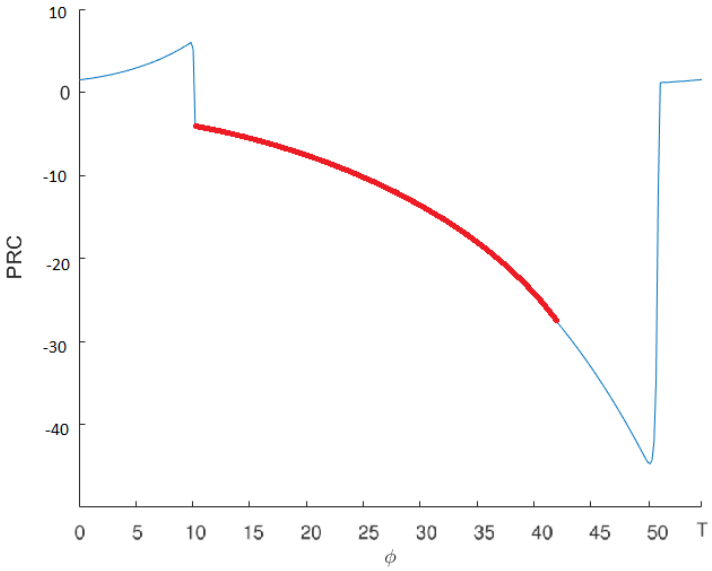

Figure 31: Region of stability for the memristor circuit model synchronizing to an external periodic stimulus. $T = 54.73$, $y = [2, 0]$.

Of course, it will also depend on the magnitude y of the perturbation which determines the maximum and the minimum of the PRC ($PRC(t) = Z(t) \cdot y$). The condition for a fixed point to be stable is: $-2 < \text{PRC}'(\phi) < 0$, so the stability is only possible when the PRC is decreasing. But as the perturbation

decreases, the region of stability increases. Figure 31 shows a situation where $y = 2\text{V}$, and the perturbation allows a region of stability from $\phi \in (10, 45)$.

In summary, if we want to synchronize our memristor oscillation to an external stimulus, it must comply that the difference of periods must be less than the maximum and minimum of the PRC and the magnitude y of the stimulus must be such that $-2 < Z'(\phi)y < 0$.

5.2 Weak coupling of Memristors

The following sections explore different models of coupling memristors, applying to them the methods for the PRC and the interaction function described in the previous sections of this project. Let us make the same assumptions as in section 4.5 for a *weak* coupling and reproduce the results we already obtained for the neurons models.

5.2.1 Synchronization of two identical Memristors

Figures 32 and 35 show the results of applying the averaging method and obtaining the interaction function as described in section 4.5.

The first case we study is the coupling of two memristor circuits using a resistor (10) (Figure 32). The parameters used will remain the same as described in (9).

This particular memristor coupling shows an interesting behaviour, it has four equilibrium points: two of them are stable and the other two are unstable. The stable points are at $\phi = 0$ and $\phi = T/2$, so in this case it is possible to synchronize in phase (see Figure 33) or in anti-phase (see Figure 34), depending on the phase difference at the beginning.

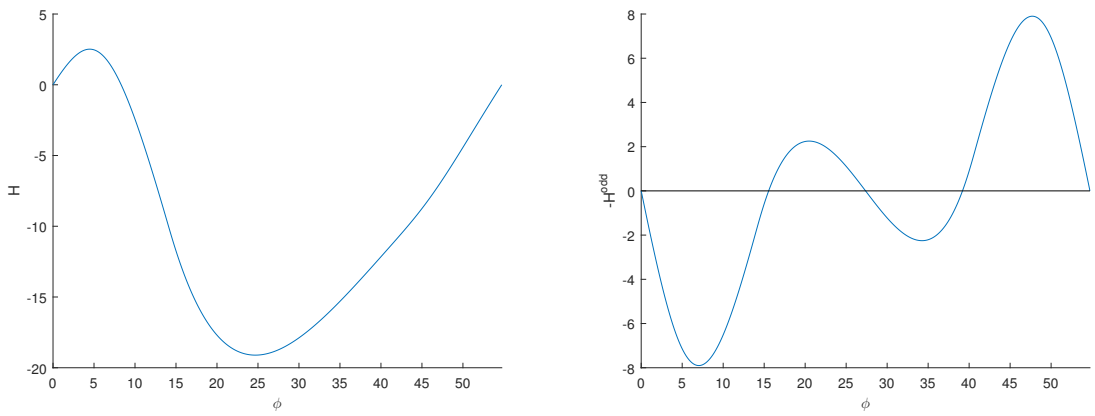

Figure 32: Interaction function H on the left and $-H^{odd}$ on the right for two memristic circuits coupled with a resistor.

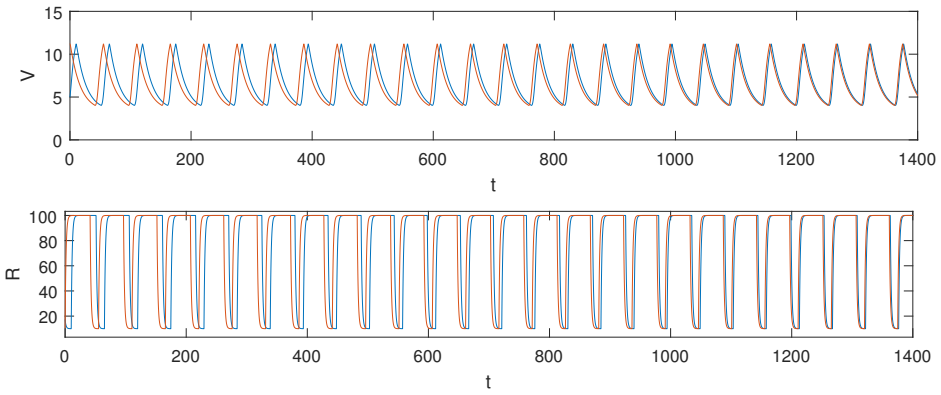

Figure 33: Solution of the two memristic circuits coupled with a resistor, with initial phase difference $\phi = 7.9$ ($T = 54.7362$). Memristors tend to a phase difference of zero (synchronization in phase).

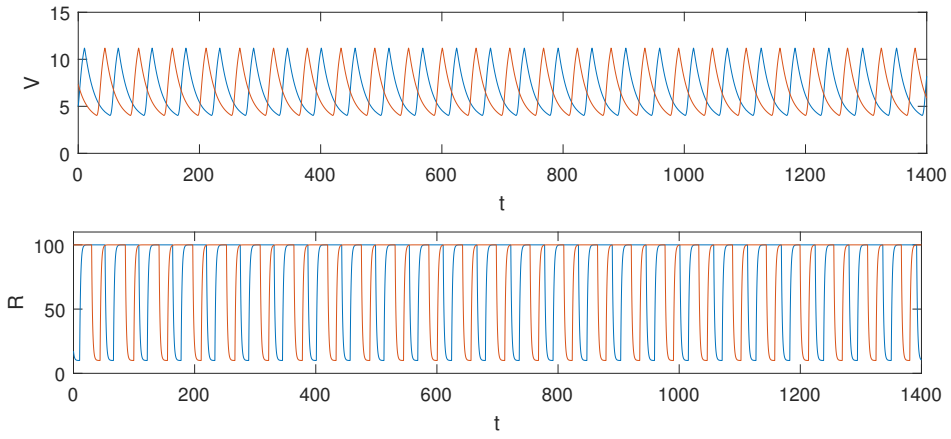

Figure 34: Solution of the two memristic circuits coupled with a resistor, with initial phase difference $\phi = 22.0379$ ($T = 54.7362$). Memristors tend to a phase difference of $T/2$ (synchronization in anti-phase).

The second case we study is the coupling of two memristor circuits using a capacitor (11) (Figure 35). The dynamics shows only one stable fixed point at $\phi = T/2$ and another one unstable at $\phi = 0$, meaning that the memristors synchronization is in anti-phase.

If we make an analogy with the results for neurons, coupling memristors with a resistor provides similar results to the excitatory coupling because it allows synchonization in phase, while coupling memristors with a capacitor is similar to the inhibitory coupling since it allows synchronization in anti-phase.

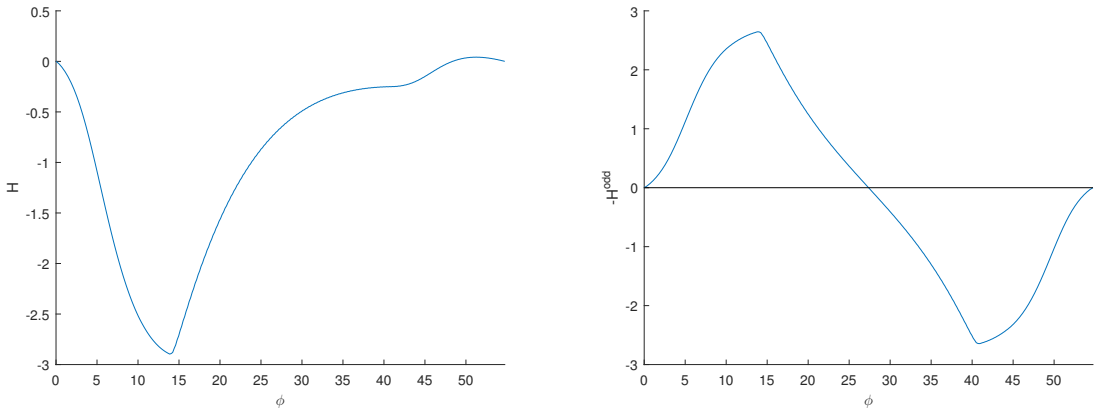

Figure 35: Interaction function H on the left and $-H^{odd}$ on the right for the memristors model coupled using a capacitor.

5.2.2 Synchronization of two non-identical Memristors

Consider that the memristor devices follow the same model but with a slight difference in their periods. Then, we can study the dynamics when coupled by applying the method of section 4.6.1. Results for the capacitor coupling (see Figure 37) are the same as in the inhibitory case for neurons, that is, there is a range of values for $\Delta\omega$ where two fixed points always exist delimited by two saddle-node bifurcations. For the resistor coupling (see Figure 36), results are also similar but with a region of four fixed points, also delimited by its local maximum and minimum by a saddle-node bifurcation.

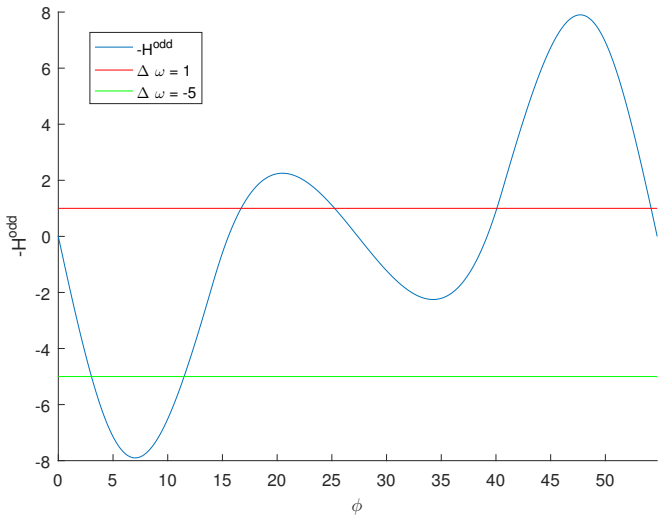

Figure 36: Resistor coupling for the memristor model with non-identical oscillators, with two different values for $\Delta\omega$.

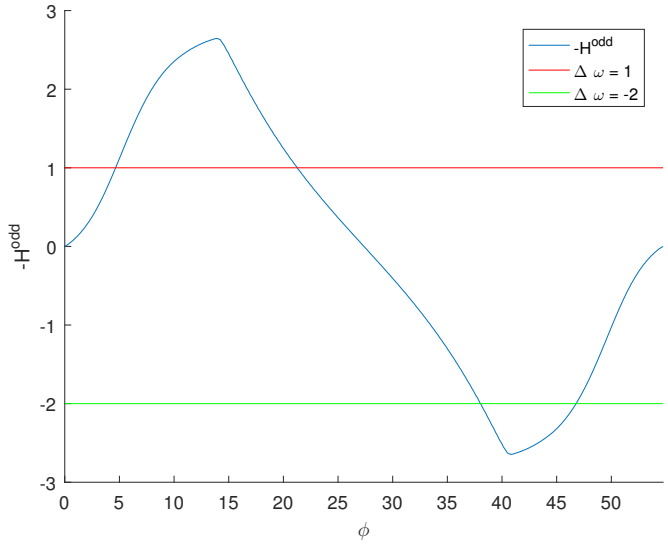

Figure 37: Capacitor coupling for the memristor model with non-identical oscillators, with two different values for $\Delta\omega$.

5.2.3 Synchronization of three Memristors

In this section we consider three memristor circuits all-to-all coupled using resistors or capacitors and we will apply the method explained in section 4.7. We. Figure 39 shows a schematic representation of that coupling.

Figures 38 and 40 show the nullclines for equations (41) for the case of a three memristor circuit with resitor and capacitor couplings respectively. The explicit expression for equations has been computed interpolating the interaction H using the FFT.

As before, resistor coupling and capacitor coupling remain analogous to the excitatory and inhibitory synaptic coupling for neurons, respectively. The main difference is for the model with capacitors, where more equilibrium points appear. Other than that, the equilibrium points have a correspondence from memristors to neurons even with the stability properties. There is a summary of the equilibrium points for the memristors model in table 3 for resistors and table 4 for capacitors.

Table 3: Fixed points for the 3 memristor coupled with resistors model. T= 54.73624

Point: (ψ_1, ψ_2)	Eigenvalues of the Jacobian	Type	Comments
(0,0)	-0.24674, -0.24674	Stable node	The memristors will synchornize in phase as expected from excitatory coupling.
(T/3,T/3)	0.08485+0.25149i, 0.08485-0.25149i	Unstable focus	The memristors will not synchronize with the same phase difference between them.
(0, 43.24493)	0.30353, -0.30972	Saddle	Memristors 1 and 2 synchronize in phase, memristor 3 does not.
(T-43.24493,0)	0.30353, -0.30972	Saddle	Memristors 2 and 3 synchronize in phase, memristor 1 does not.
(43.24493,T-43.24493)	0.30353, -0.30972	Saddle	Memristors 1 and 3 synchronize in phase, memristor 2 does not.

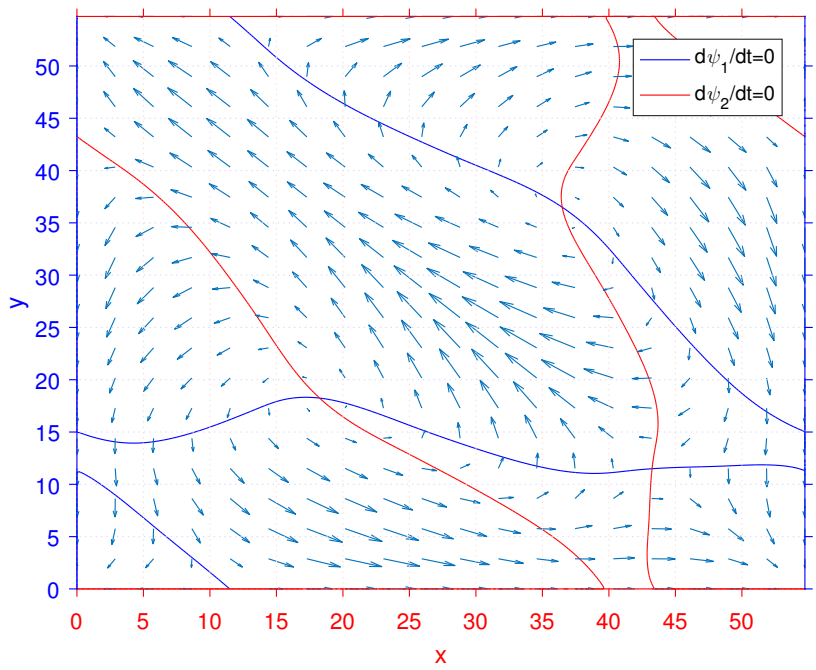

Figure 38: Nullclines of the system (41) for a model of three memristors coupled with resistors. The intersection of the nullclines determines the equilibrium points.

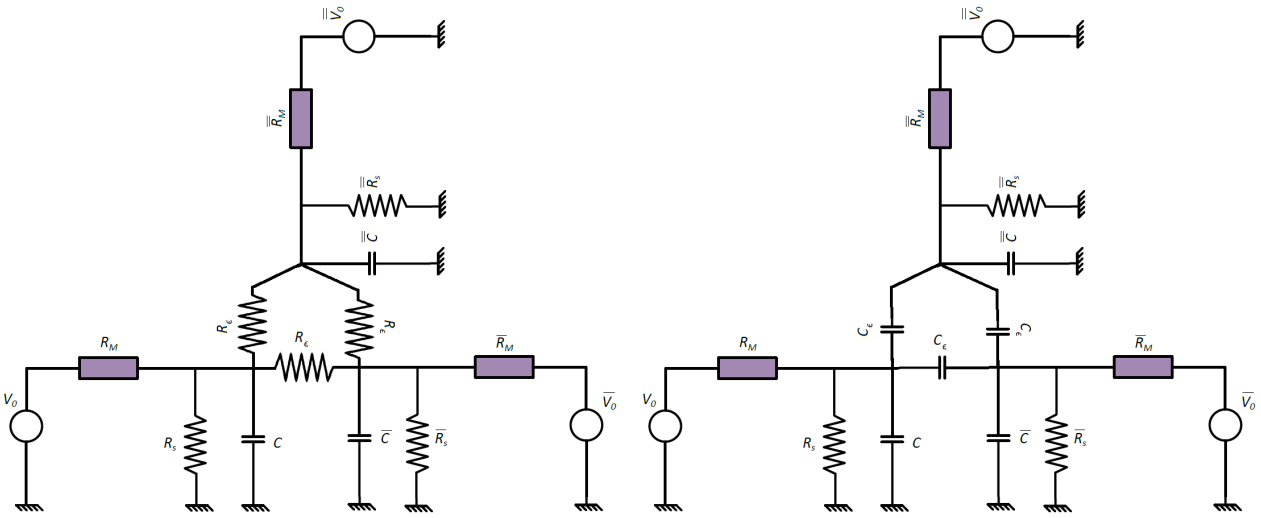

Figure 39: Schematic representation of three memristor circuits coupled using resitors (left) or capacitors(right).

Table 4: Fixed points on the 3 memristor coupled with capacitors model. T= 54.73624

Point: (ψ_1, ψ_2)	Eigenvalues of the Jacobian	Type	Comments
(0,0)	0.05522, 0.05522	Unstable node	The memristors will synchornize in phase as expected from excitatory coupling.
(T/3,T/3)	-0.04115+0.01174i, -0.04115-0.01174i	Stable focus	The memristors will not synchronize with the same phase difference between them.
(0, 24.35090)	0.01717, -0.04645	Saddle	Memristors 1 and 2 synchronize in phase, memristor 3 does not.
(T-24.35090,0)	0.01717, -0.04645	Saddle	Memristors 2 and 3 synchronize in phase, memristor 1 does not.
(24.35090,T-24.35090)	0.01717, -0.04645	Saddle	Memristors 1 and 3 synchronize in phase, memristor 2 does not.
(0.97229, 23.99195)	0.01791, -0.04668	Saddle	All memristors out of phase. 1 and 2 are close, and 3 has a greater phase difference.
(T-23.99195-0.97229, 0.97229)	0.01791, -0.04668	Saddle	All memristors out of phase. 2 and 3 are close, and 1 has a greater phase difference.
(23.99195, T-23.99195-0.97229)	0.01791, -0.04668	Saddle	All memristors out of phase. 1 and 3 are close, and 2 has a greater phase difference.

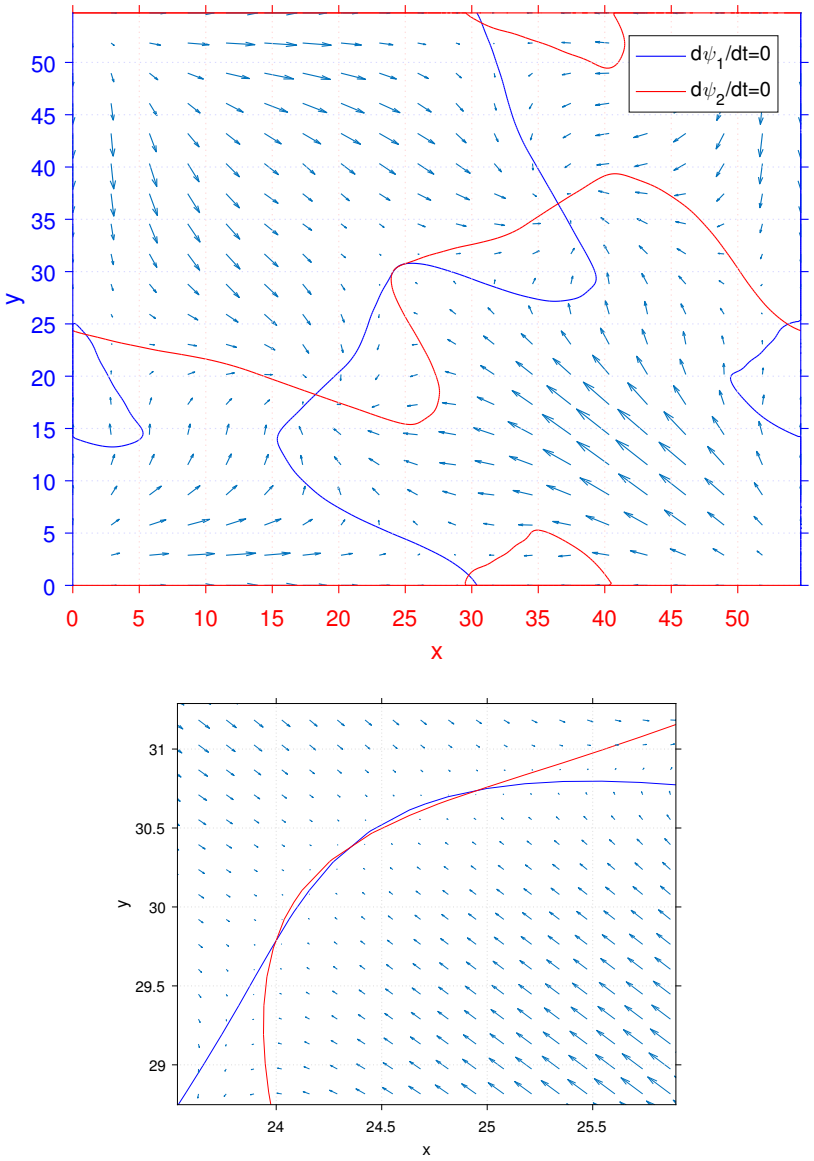

Figure 40: Top: Nullclines of the system (41) for a model of three memristors coupled with capacitors. The intersection of the nullclines determines the equilibrium points. Bottom: Close-up of a region with 3 fixed points.

6 Conclusion

In this project, we formulated a new model for electrical oscillators with a memristic component such as Vanadium dioxide. The model takes a new perspective from previous modellings, because it considers the resistance of the memristic device as important as the rest of the oscillatory dynamics. Similarly to results in neuroscience, oscillation is now explained as bifurcations of the equilibrium points due to the fast-slow dynamics of the resistance and voltage. What came out of this formulation is a model than resembles that of the neurons', giving us the opportunity to apply all the methodology known for this field.

The first application we found is how a memristic circuit would behave subject to an external periodic stimulus, and the results would explain under which circumstances we will get a synchonization to a certain frequency in the laboratory. Following results show that the devices can interact between them and change their phases, usually ending in states where they synchronize in phase or anti phase. Future studies of the interaction should include a n-memristor model, that would show a full perspective of how "information" in the form of phase can be exchanged between oscillators. A system of this kind could led to processors with non-boolean computation, replacing the common bit by oscillators. A computer working with this technology would resemble the human brain, because neurons and memristic circuits have similar oscillation characteristics.

Experiments using the results of this project are being coordinated by Dr. Ferran Macià from the MULFOX group of the ICMAB led by Dr. Josep Fontcuberta (`https://departments.icmab.es/mulfox/`).

A Appendix: Bifurcations in Equilibrium Points

Bifurcation theory is concerned with how solutions change as parameters in a model are varied. For example, this project exposed how the parameters of the Morris Lecar model or the memristor circuit equations allow different kinds of fixed points and periodic orbits. There are many kinds of bifurcations, and the ones that appeared are the Andronov-Hopf and the Saddle-Node bifurcations.

A.1 Saddle-Node Bifurcation

Saddle-node or fold bifurcation is a local bifurcation in which two fixed points of a dynamical system collide and annihilate each other.

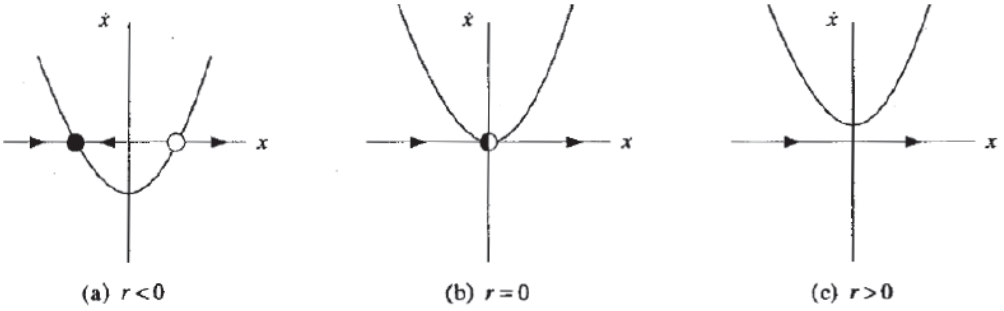

Figure 41: Saddle-node bifurcation of $\frac{dx}{dt} = r + x^2$.

A.2 Andronov-Hopf Bifurcation

The appearance or the disappearance of a periodic orbit through a local change in the stability properties of a steady point is known as the Hopf bifurcation. The bifurcation can be supercritical or subcritical, resulting in stable or unstable limit cycle, respectively.

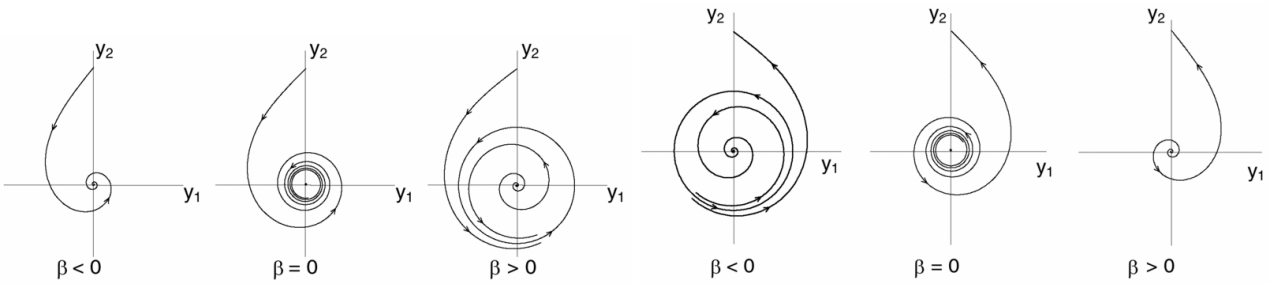

Figure 42: Supercritical (right) and subcritical (left) Hopf bifurcations.

A.3 The Canard Phenomenon

Canards are a phenomenon occurring in singularly perturbed systems (also known as slow-fast systems). The classical canard phenomenon explains the very fast transition upon variation of a parameter from a

small amplitude limit cycle via canard cycles to a large amplitude relaxation cycle. This very fast transition called canard explosion happens within an exponentially small range of a control parameter.

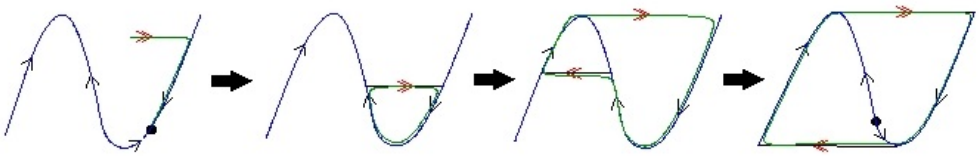

Figure 43: Example of the Canard phenomenon.

B Appendix: The Averaging method

Consider a system of the form:

$$\dot{y} = \epsilon f(y, t, \epsilon); \quad y \in U \subseteq \mathbb{R}^n, \quad \epsilon << 1 \tag{42}$$

where $f : \mathbb{R}^n \times \mathbb{R} \times \mathbb{R}^+ \to \mathbb{R}^n$ is C^r, $r \geq 1$, bounded on bounded sets, and of period $T > 0$ in t; U is bounded and open. The associated autonomous averaged system is defined as:

$$\bar{y}' = \epsilon \frac{1}{T} \int_0^T f(\bar{y}, t, 0) dt \equiv \epsilon \bar{f}(\bar{y}). \tag{43}$$

The original system (42) can be approximated by the averaged system (43) through the following theorem.

Theorem B.1. (The Averaging Theorem) *There exists a C^r change of coordinates $y = \bar{y} + \epsilon w(\bar{y}; t; \epsilon)$ under which (42) becomes*

$$\dot{\bar{y}} = \epsilon \bar{f}(\bar{y}) + \epsilon^2 f_1(\bar{y}, t, \epsilon), \tag{44}$$

where f_1 is of period T in t.

A proof of the theorem can be found in [16].

C Appendix: Interpolation with Fast Fourier Transform

The fast Fourier transform (FFT) can be used to estimate the coefficients of a trigonometric polynomial that interpolates a set of data.

The FFT algorithm is associated with applications in signal processing, but it can also be used more generally as a fast computational tool in mathematics. While studying asteroid orbits in the early 19th century, Carl Friedrich Gauss discovered a mathematical shortcut for computing the coefficients of a polynomial interpolant by splitting the problem up into smaller subproblems and combining the results. His method was equivalent to estimating the discrete Fourier transform of his data.

Given x_n, $n = 0, ...N-1$ equidistant values of H, the FFT finds the coeficients:

$$C_k = \frac{1}{N}\sum_{n=0}^{N-1} x_n e^{-i2\pi k\frac{n}{N}}, \qquad k = 0, \dots, N-1. \tag{45}$$

At this point, we can just select the first M coeficients, neglecting smaller values. With this, we can interpolate and get a continuous solution in the form:

$$H(\psi) = \sum_{n=0}^{M-1} C_k e^{-i2\pi n\frac{\psi}{T}}. \tag{46}$$

D Appendix: Relevant MATLAB code

The following code is used for compute some of the methods explained in section 4.3, not adding miscellaneous code (for model equations, numerical integration, ODE solving...).

D.1 Poincaré map using Newton's method

```
function [t_final, p_final] = poincare_section(ci,j,section,tol)
    % Calculates de Poincaré Mapping of 'ci'
    % Find the j-th cross with the poincare section "x_2 = section"
    %using ci as initial condition.

    if nargin < 4, tol = 1.e-12; end
    t = 100; %integration time
    %Looking for first time approximation
    [T,Y] = ode78(@model,[0,t],ci);
    pos = length(Y(:,1));
    cont = 0;
    for i = 2:length(Y(:,1))
        if (Y(i,2)-section)*(Y(i-1,2)-section)<0
            cont = cont+1;
        end
        if cont == abs(j)
            pos = i;
            break
        end
    end
    ti = T(pos); % Time approximation
    % Newton's method
    for i=1:30
        [~,Y1] = ode78(@model,[0,ti],ci,0,tol);
        Gti = Y1(end,2)-section;
        if abs(Gti)<tol break; end
        model_i = model(ti,Y1(end,:));
```

```
        dGti = model_i(2);
        ti = ti - Gti/dGti;
    end
    t_final = ti;
    p_final = Y1(end,:);

end
```

D.2 Periodic orbits using Poincaré sections and bisection method

```
function [ORB,TIME]=Periodic_Orbit(tol)
    if nargin < 1, tol = 1.e-12; end
    %Interval for the P.O., Xin =(-30,-0.3), Xout = (-20,0.3)
    v = [-30,-20];
    %Poincaré section
    w = 0.3;
    section = w;
    DX = zeros(1,n);
    %Find Poincaré sections for Xin and Xout
    for k=1:length(v)
        ci =[v(k), w];
        [t, p] = poincare_section(ci,2,section,tol);
        DX(k) = p(1);
    end
    %Bisection method
    [x,t_orbit] = bisection(v(k-1),DX(k-1),v(k),DX(k));
    ORB = [x;w];
    TIME = t_orbit;
%%%%%%%%%%%%%%%%%%%%%%%
%Bisection method
    function [resul,tt2] = biseccio(x1, section_x1, x3, section_x3)
    % Method that finds the point x2 between x1 and x3 (with mapping at
    % section_x1, section_x3) that satisfies (x2 - section_x2) < tol
        for q=1:50
            x2 = (x1+x3)/2;
            result = x2;
            ci2 =[x2, section];
            [t2, p2] = poincare_section(ci2,2,section,tol);
            section_x2 = pp2(1);
            if(abs(section_x2-x2)<tol) break; end
            if((section_x1-x1)*(section_x2-x2)<0)
                x3 = x2;
                section_x3 = section_x2;
            else
                x1 = x2;
                section_x1 = section_x2;
```

```
            end
        end
    end
end
```

D.3 PRC and interaction H using the variational method

```
%Discretization of the PRC
n_prc = 100;
%Calculate the periodic orbit of the system
[ORB,TIME]=Periodic_Orbit();
v=ORB(1); w=ORB(2);
c_ini = [v,w,1,0,0,1];
%Integrate the variational equations
[~,Y] = ode78(@model_variational,[0,TIME],c_ini,0,tol);
YT = [Y(end,3), Y(end,4); Y(end,5), Y(end,6)];

%Get eigenvalue and eigenvector
[V,D] = eigs(YT);
if(abs(D(1,1)-1)<1e-8)
    V_one = V(:,1); V_small = V(:,2);
    lambda = D(2,2);
else
    V_one = V(:,2); V_small = V(:,1);
    lambda = D(1,1);
end

%Initialize variables
t = linspace(0,TIME,n_prc);
VW = zeros(2,n_prc); S = zeros(1,n_prc);
K = zeros(2,n_prc); Z = zeros(2,n_prc);
J = [0,-1;1,0];
%Computing PRC for each point of the discretization
for i=1:n_prc
    [~,Y] = ode78(@model_variational,[0,t(i)],c_ini,0,tol);
    vw = [Y(end,1), Y(end,2)];
    Yt = [Y(end,3), Y(end,4); Y(end,5), Y(end,6)];
    % Applying Proposition 4.3.4
    K(:,i) = exp(lambda*t(i)/TIME)*Yt*V_small;
    Z(:,i) = J*K(:,i)/dot(J*K(:,i), model(t(i),vw));

    %Saving values of S for Interation%%
    VW(:,i) = vw;
    [~,Y] = ode78(@model,[0,t(i)],[v,w,0.053729],0,tol);
    S(i) = Y(end,3);
end
```

```
%Infinitesimal PRC (Z)%%%%%%%%%%%%%%
Z_function = Z
%%%%%%%%%%%%%%%%%%%%%%%%%%%%%%%%%%%
%Computing the Interaction H from the PRC
%Initialization
c = 20
h = TIME/(n_prc-1);
Vsyn = 120; %Choosing excitation (120) or inhibition (-75)
H = zeros(1,n_prc);
%Remove last point because of periodicity (0==T)
Z_aux  = Z_FUNCTION(:,1:end-1); VW_aux = VW(:,1:end-1); S_aux = S(1:end-1);

for i=1:n_prc-1
    % Computing the value inside the integral for n_pcr-1 equidistant points
    ZG = Z_aux(1,:).*circshift(S_aux',-(i-1))'.*(Vsyn-VW_aux(1,:))/c;
    %Computing the integral using Newton cotes' 4/90 rule
    H(i) = (1/TIME)*cotes(ZG,h,5);
end
H(end) = H(1);

%Interaction function%%%%%%%%%%%%%%%
H_function = H
%%%%%%%%%%%%%%%%%%%%%%%%%%%%%%%%%%%
```

E Bibliography

References

[1] S. Datta, N. Shukla, M. Cotter, A.Parihar, A. Raychowdhury, *Neuro Inspired Computing with Coupled Relaxation Oscillators*, 2014 51st ACM/EDAC/IEEE Design Automation Conference (DAC), San Francisco, CA, 2014, pp. 1-6.

[2] N. Shukla, A. Parihar, E. Freeman, *Synchronized charge oscillations in correlated electron systems* Scientific Reports 4 : 4964, 2014.

[3] A. Pergament, A. Crunteanu, A. Beaumont, G. Stefanovich.*Vanadium Dioxide: Metal-Insulator Transition, Electrical Switching and Oscillations. A Review of State of the Art and Recent Progress*, EMN Meeting on Computation and Theory, Energy Materials and Nanotechnology, November 9 to 12, 2015, Istanbul, Turkey.

[4] P. Maffezzoni, L. Daniel, N. Shukla, S. Datta, A. Raychowdhury, *Modeling and simulation of vanadium dioxide relaxation oscillators*, IEEE Trans. Circuits Syst. I, Reg. Papers, vol. 62, no. 9, pp. 2207–2215, Sep. 2015.

[5] G.B. Ermentrout, D.H. Terman.*Mathematical foundations of neuroscience*, Springer, New York, 2014.

[6] F.C. Hoppensteadt, E.M. Izhikevich. *Weakly Connected Neural Networks*, Springer, New York, 2012.

[7] G.B. Ermentrout. *Simulating, Analyzing, and Animating Dynamical Systems A Guide to Xppaut for Researchers and Students.*, Society for Industrial and Applied Mathematics, Philadelphia, 2002.

[8] D.B. Strukov, G.S. Snider, D.R. Stewart, R.S. Williams *The missing memristor found* Nature volume 453, 2008, pp. 80–83.

[9] J. Guckenheimer, *Isochrons and phaseless sets*, J. Math. Biol., 1 (1974/75), pp. 259-273.

[10] D. Hansel, G. Mato, C. Meunier *Synchrony in Excitatory Neural Networks* Neural Computation 7, 307-337, Massachusetts Institute of Technology, 1995.

[11] Y. Kuramoto. *Chemical Oscillations, Waves, and Turbulence*, volume 19, Springer Series in Synergetics. Springer, Berlin, 1984.

[12] A. Guillamon, G. Huguet. *A Computational and Geometric Approach to Phase Resetting Curves and Surfaces*, Society for Industrial and Applied Mathematics, 2009, pp. 1040-1041.

[13] V. Novicenko, K. Pyragas *Computation of phase response curves via a direct method adapted to infinitesimal perturbations* Nonlinear Dyn, Springer, 2012.

[14] E. Brown, J.Moehlis, P. Holmes *On the Phase Reduction and Response Dynamics of Neural Oscillator Populations*, Neural Computation 16, 673–715 Massachusetts Institute of Technology, 2004.

[15] E.M. Izhikevich. *Dynamical Systems in Neuroscience: The Geometry of Excitability and Bursting.*, Computational Neuroscience, MIT Press, Cambridge, MA, 2007.

[16] C. Zhang *An Introduction to Averaging Method*, Dynamics at the Horsetooth Volume 2A, 2010.